TIME FILTERS FOR NUMERICAL WEATHER PREDICTION

by

Yong Li

Bachelor of Science in Mathematics,

University of Science and Technology of China, Hefei, China, 2009

Master of Philosophy in Mathematics,

The Chinese University of Hong Kong, Hong Kong, 2011

Submitted to the Graduate Faculty of

the Kenneth P. Dietrich School of Arts and Sciences in partial fulfillment

of the requirements for the degree of

Doctor of Philosophy

University of Pittsburgh

2016

UNIVERSITY OF PITTSBURGH

DIETRICH SCHOOL OF ARTS AND SCIENCES

This dissertation was presented

by

Yong Li

It was defended on

April 28, 2016

and approved by

Prof. Catalin Trenchea, Dept. of Mathematics, University of Pittsburgh

Prof. William Layton, Dept. of Mathematics, University of Pittsburgh

Prof. Michael Neilan, Dept. of Mathematics, University of Pittsburgh

Prof. Noel Walkington, Dept. of Mathematical Sciences, Carnegie Mellon University

Dissertation Advisors: Prof. Catalin Trenchea, Dept. of Mathematics, University of Pittsburgh,

Prof. William Layton, Dept. of Mathematics, University of Pittsburgh

TIME FILTERS FOR NUMERICAL WEATHER PREDICTION

Yong Li, PhD

University of Pittsburgh, 2016

The Robert–Asselin (RA) time filter combined with leapfrog scheme is widely used in numerical models of weather and climate. The RA filter suppresses the spurious computational mode associated with the leapfrog method, and successfully stabilizes the numerical solution. However, it also weakly dampens the physical mode and degrades the formal second-order accuracy of the leapfrog scheme to first order. There is a natural intention to reduce the time-stepping error as it has proven to be a substantial part of the total forecast error. Yet a new scheme must be non-intrusive, i.e., easily implementable in legacy codes in order to avoid significant programming undertaking.

The object of this work is the development, analysis and validation of novel Robert–Asselin type time filters, addressing both of the above problems. Specifically, we first propose and analyze a higher-order Robert–Asselin (hoRA) type time filter. The analysis reveals that the filtered leapfrog scheme exhibits second- or third-order accuracy depending on the filter parameter. We then investigate its behavior when used in conjunction with the implicit-explicit integration, which is commonly used in weather and climate models to relieve the severe time step restriction induced by unimportant high-frequency waves. Next, we build a framework of constructing a family of hoRA filters with any pre-determined order of accuracy. In particular, we focus on the fourth-order time filter. Finally, we present supplemental analysis for several filters developed by Williams. For each direction, we present comprehensive error and stability analysis, and perform numerical tests to verify theoretical results.

Keywords: numerical weather prediction, time filters, Robert–Asselin–Williams, higher-order Robert–Asselin, leapfrog scheme, Crank-Nicolson, G-stability.

TABLE OF CONTENTS

LIST OF TABLES

LIST OF FIGURES

PREFACE

I would like to express my deepest gratitude to my dissertation advisor, Professor Catalin Trenchea, for his guidance and support throughout my graduate studies at University of Pittsburgh. I thank him for his inspiring discussions, sound advice, and constant encouragement towards my research. Outside mathematics, he is a great friend and life mentor. I have enjoyed every moment we spent together in the last several years. It is my greatest honor and luck in my life to have him as my advisor.

I wish to thank my co-advisor Professor William Layton for his generous support, helpful advice and invaluable guidance on my research. His contagious enthusiasm, profound knowledge, and unique perspective about research and mathematics have greatly helped me carry out this thesis.

I also want to thank Professors Michael Neilan and Noel Walkington for serving on my committee and for being available to discuss about my research. I am grateful to their valuable comments and suggestions.

I would like to thank Dr. Mike Sussman for his stimulating and enthusiastic lectures, from which I have learned most of my programming skills. I also thank him for his willingness to discuss and give helpful comments on my research.

I wish to thank Professors Paul Williams (University of Reading), Dale Durran (University of Washington), Hilary Weller (University of Reading) and Assad Oberai (Rensselaer Polytechnic Institute) for their inspiring discussions and kind willingness to provide help on my research.

A big thanks goes to all my fellow graduate students at University of Pittsburgh, and especially to Nick Hurl, Nan Jiang, Sarah Khankan, Marina Moraiti, Ali Pakzad, Aziz Takhirov, Hoang Tran and Xin Xiong.

Finally, I thank my family, especially my parents, Hengshu and Guanghao, my sister Ji Eun, and my parents in-law for their endless love and constant support. Most of all, I thank my beloved wife, Lina. Without her support, this work would not have been completed. I dedicate this dissertation to her.

1.0 INTRODUCTION

The possibility of deterministic weather prediction was suggested by Vilhelm Bjerknes as early as 1904. Later, Lewis Richardson attempted to produce such a forecast by manually integrating a finite-difference approximation to the equations governing atmospheric motion. However, his calculations did not yield a reasonable forecast, and moreover, the human labor required to obtain this disappointing result was so great that subsequent attempts at deterministic weather prediction had to await the advent of the computer and computer simulations that the computation's time was reduced to less than the forecast period itself. The ENIAC was used to create the first weather forecasts via computer in 1950, based on a highly simplified approximation to the atmospheric governing equations. Its success led to the rapid growth of a new meteorological subdiscipline, "numerical weather prediction". These early efforts in numerical weather prediction began a long collaboration between numerical analysts and atmospheric scientists. The use of numerical models in atmospheric and oceanic science has subsequently expanded into almost all areas of active research.

From a functional perspective, the task of predicting future weather and climate may be reduced to the following iterative procedure. First, given the state of the atmosphere, ocean, and other earth-system components at any time (the input), use the governing equations to compute the state at a slightly later time (the output). Then, repeat the loop as many times as required, always using the previous output as the next input. This prediction framework presents some form of error compared to what the atmosphere will actually do. Typically, the forecast errors come from uncertainty in the initial states, boundary conditions, forcing, and the numerical model (model errors and numerical errors). The latter contains physical and dynamical assumptions, parameterizations of subgrid processes, spatial emsh approximations, and the discrete time-stepping error. The impact of time-stepping schemes

on the climate modes has been studied in the literature, (e.g., [36, 45, 55]). Teixeira et al. [45] mentioned that "*In the weather and climate prediction community, when thinking in terms of model predictability, there is a tendency to associate model error with the physical parameterizations. In this paper, it is shown that time truncation error... can be a substantial part of the total forecast error*". Therefore, selecting a proper time-stepping method becomes significantly important. In this thesis, we dedicate ourselves to the development and analysis of non-intrusive higher-order time-stepping schemes.

Among many different time-stepping methods, the *leapfrog* scheme emerged, from the early years of numerical weather prediction, as the method of choice and is still popular for a number of reasons. Perhaps the most important attribute of the leapfrog scheme is that it preserves exactly the amplitude of a pure oscillation. The dissipative characteristics of other time integration schemes are generally too strong, while the absence of computational damping of leapfrog scheme is especially desirable for long-time integrations. Another feature of the leapfrog method is efficiency, namely, it evaluates the right-hand side of the meteorological tendency equations only once per time step, in contrast with most other schemes. The leapfrog scheme applied to a generic differential equation

$$\frac{du}{dt} = F(u)$$

is given by

$$u^{n+1} = u^{n-1} + 2\triangle t F(u^n),$$

where $\triangle t$ is the time step and u^n is the approximated solution at time $t^n := n\triangle t$.

The leapfrog method is a three-time-level scheme, and when applied to a simple set of linear differential equations, it generates two modes of motion. One is the *physical* mode, which contributes to the true solution, while the other one is the *computational* mode, which is merely artificial and has no relation to the differential equations that are being integrated. The computational mode of the leapfrog scheme is undamped in linear problems, meaning that it preserves the amplitude in each time step. In nonlinear problems, however, the nonlinear terms introduce couplings between the physical and computational modes which may amplify the computational mode. In short-time simulations of weather and climate,

the growth of the computational mode is generally hard to detect, but when long-time integrations are considered, the computational mode dominates the solution.

One possible approach to control the leapfrog scheme's computational mode is to periodically use a two-time-level scheme, e.g., a Matsuno step after every 11 leapfrog steps [36]. The idea is to reset the amplitude to zero periodically, so it never becomes large enough/problematic. Another technique is to use different explicit time-stepping schemes, e.g., the second-order Adams-Bashforth method [32], the third-order Adam-Bashforth [10], the leapfrog-trapezoidal method [23, 54] or the Magazenkov method [34].

The ubiquitous strategy in atmospheric models, for controlling the leapfrog scheme's computational mode, is the non-intrusive implementation of a time filter after each leapfrog time step. Robert [40] designed such a filter, which Asselin [4] analyzed and proved to effectively damp the computational mode of the leapfrog scheme. This time filter is referred to as the Robert–Asselin (RA) filter. The RA-filtered leapfrog scheme is

$$v^{n+1} = u^{n-1} + 2\triangle t F(v^n), \tag{1.1}$$

$$u^n = v^n + \frac{\nu}{2}\left(v^{n+1} - 2v^n + u^{n-1}\right), \tag{1.2}$$

where v and u denote the unfiltered (provisional) and filtered (definitive) variables, respectively. The dimensionless parameter $\nu \in [0, 1]$ determines the strength of the filter, i.e., ν controls the computational mode of the leapfrog scheme.[1]

The accuracy and stability properties of the RA filter were investigated in [5, 6, 8, 9, 13, 16, 20, 39, 43, 48]. Currently, the RA filter is used in operational numerical weather prediction models, atmospheric general circulation models for climate simulation, ocean general circulation models, and models of fluids in rotating annulus laboratory experiments, etc. A comprehensive list of atmospheric models with RA filter can be found in [48]. The RA filter, however, also damps the physical mode. As a result, the formal second-order accuracy of the leapfrog scheme is reduced to first order, and can degrade the accuracy of model simulations. Therefore, physical quantities (e.g., energy, mass) conserved by the time-continuous equations are not necessarily conserved by time-discretized equations when the filter is used.

[1] A value of $\nu = 0.12$ is typically used in the NCAR community climate model [51]; $\nu = 0.4$ is common in mesoscale convective models; Schlesinger et al. [43] recommend a value of ν in the range of $0.5 - 0.6$ for general advection-diffusion modeling.

In this thesis, we propose and analyze hoRA type time filters: hoRA2 (Chapter 2), hoRA3(Chapter 2), and hoRA4 (Chapter 4). The hoRA2(3) filter combined with the leapfrog scheme exhibits second- or third-order accuracy depending on the value of the filter parameter. We present several numerical tests, including simple pendulum [50], Lorenz system [10], and the Ozone photochemistry [11], to confirm its outperformance compared with existing time filters, RA and RAW filters. We then investigate the accuracy and stability properties of the hoRA2(3) filter when used in conjunction with the implicit-explicit integration, which is commonly used in weather and climate models to relieve the severe time step restriction induced by unimportant high frequency waves (e.g., sound or gravity waves). The method is implemented in the elastic pendulum [33, 49] and the acoustic advection problem [42] to verify the theoretical results. Next, we build a framework of constructing the family of hoRA filter with any pre-determined order of overall accuracy. Following this framework, we recover the RA and hoRA2(3) filters, and in particular, we develop a fourth-order filter, hoRA4. We perform the error and stability analysis of the hoRA4-filtered leapfrog scheme, and present several numerical experiments (pure oscillation [48] and Lorenz system [10]) to verify the convergence. The family of hoRA type filters are non-intrusive linear post-process to the leapfrog step, and thus they are easy implementable in any legacy codes. Finally, we present supplemental analysis for schemes proposed by Williams in [48, 50].

The work of this thesis is based on [20, 25, 27, 28, 29, 30, 31].

2.0 A HIGHER-ORDER ROBERT–ASSELIN TYPE TIME FILTER

In this chapter, we propose and analyze a higher-order Robert-Asselin (hoRA) type time filter, a non-intrusive linear post process to the leapfrog scheme:

$$v^{n+1} = u^{n-1} + 2\triangle t F(v^n), \tag{2.1}$$

$$u^n = v^n + \frac{\beta}{2}(v^{n+1} - 2v^n + u^{n-1}) - \frac{\beta}{2}(v^n - 2u^{n-1} + u^{n-2}), \tag{2.2}$$

where the dimensionless parameter β is in the interval $[0, 1)$. Here v and u denote the unfiltered and once-filtered values, respectively.

We show that the proposed scheme improves the first-order truncation error of RA filter to at least second order. Moreover, the truncation error becomes third order for a particular value of the filter parameter β, yielding third-order accuracy for the amplitude and fourth-order accuracy for the phase speed of the physical mode (we denote this filter as hoRA2(3) to distinguish from the fourth-order hoRA filter, hoRA4, that will be discussed in Chapter 4). We present several numerical tests, including simple pendulum [50], Lorenz system [10], and the Ozone photochemistry [11], to confirm its outperformance compared with existing time filters, RA and RAW filters. The work of this chapter is based on [27]

2.1 NOTATION AND PRELIMINARIES

The stability condition, amplitude, phase-speed, and the consistency errors are illustrated by analyzing solutions to the pure oscillation equation (see e.g., [10, 11])

$$\frac{du}{dt} = i\omega\, u, \tag{2.3}$$

where i is the imaginary unit, and ω a real constant. Define the *amplification factor* A as the ratio of the approximate solution at two adjacent time steps, i.e., $A = u^{n+1}/u^n$. Throughout the text, we will denote the time step as $\triangle t$, the exact solution u at time $t^n = n\triangle t$ as $u(t^n)$, and the numerical solution approximating $u(t^n)$ as u^n. The amplification factor yields information on two quantities of interest: the amplitude and the relative phase change (phase speed) per time step. Specifically, A can be expressed in modulus-argument form $A = |A|e^{i\theta}$, where

$$|A| = \sqrt{Re(A)^2 + Im(A)^2}, \quad \theta = \tan^{-1}(Im(A)/Re(A)).$$

For the true solution to the oscillation equation (2.3), the *exact amplification factor* $A_e = e^{i\omega\triangle t}$ has unity magnitude and phase change $\omega\triangle t$ over a time interval $\triangle t$. The amplitude errors are defined as the difference between the magnitude of the approximated amplification factor $|A|$ and the correct value of unity. When $|A| = 1$, the scheme is *neutral*, if $|A| < 1$, the scheme is *damping* (stable), and if $|A| > 1$, it is *amplifying* (unstable). The relative phase change or the phase speed, on the other hand, is measured by the ratio of the phase change of the numerical scheme per time step divided by the phase change of the true solution over the same time interval, and is denoted by $R = \theta/\omega\triangle t$. The phase-speed errors are defined as the difference between the phase speed R and the unity over a time interval $\triangle t$. When $R > 1$, the method is *accelerating*, and if $R < 1$, it is *decelerating*. Unlike the amplitude, the phase change does not influence the stability of the numerical solution. Yet the phase errors accumulate and result in large simulation errors over a long time period of integration.

It is helpful to describe the relationship between the overall truncation error of an ordinary differential equation solver and the amplitude and phase-speed errors introduced by that solver when it is used to model non-dissipative oscillatory phenomena, as stated in the following result [10].

Proposition 2.1.1. *If the oscillation equation (2.3) is integrated using a linear finite-difference scheme and if the truncation error of the resulting finite-difference approximation to the oscillation equation is order p, then as $\omega\triangle t \to 0$ the amplitude in the numerical*

solution is

$$1 + \mathcal{O}[(\omega\triangle t)^n], \ \textit{where} \begin{cases} n = p+1, \ \textit{if } p \textit{ is odd;} \\ n \geq p+2, \ \textit{if } p \textit{ is even;} \end{cases}$$

and the phase speed is

$$1 + \mathcal{O}[(\omega\triangle t)^m], \ \textit{where} \begin{cases} m \geq p+1, \ \textit{if } p \textit{ is odd;} \\ m = p, \ \textit{if } p \textit{ is even.} \end{cases}$$

2.2 PREVIOUS WORK: RA AND RAW TIME FILTERS

In 2009, Williams [48] proposed a modification to the Robert–Asselin (RA) filter, which combined with the leapfrog (LF) scheme is

$$w^{n+1} = u^{n-1} + 2\triangle t F(v^n), \tag{2.4}$$

$$u^n = v^n + \frac{\nu\alpha}{2}(w^{n+1} - 2v^n + u^{n-1}), \tag{2.5}$$

$$v^{n+1} = w^{n+1} - \frac{\nu(1-\alpha)}{2}(w^{n+1} - 2v^n + u^{n-1}), \tag{2.6}$$

where w, v, and u denote the unfiltered, once filtered, and twice filtered variables, respectively. The parameter ν is as in the RA filter, and the new dimensionless parameter $\alpha \in [0.5, 1]$. The filter is now referred to as the Robert–Asselin–Williams (RAW) filter. When $\alpha = 1$ the RAW filter recovers to RA filter (1.2). Compared with RA, RAW provides higher accuracy for the amplitude of the physical mode (see Table 2.2). More precisely, the amplitude of the physical mode of LF-RAW is first-order accurate for $\alpha \in (0.5, 1]$, and of particular interest, it is third order when $\alpha = 0.5$ in which case the three-time-level mean is conserved. However, LF-RAW is unstable in this case. Thus, Williams suggests taking $\alpha \gtrapprox 0.5$, e.g., $\alpha = 0.53$ to obtain almost third-order accuracy for the amplitude of the physical mode [48]. The filter has been implemented and studied in [1, 20, 35, 38, 46, 52, 53, 49] with excellent results.

2.3 THE HIGHER-ORDER ROBERT-ASSELIN TYPE TIME FILTER

The LF scheme with hoRA2(3) time filter (2.1)-(2.2) applied to the oscillation equation (2.3) is

$$v^{n+1} = u^{n-1} + 2i\omega\triangle t\, v^n, \tag{2.7}$$

$$u^n = v^n + \frac{\beta}{2}(v^{n+1} - 2v^n + u^{n-1}) - \frac{\beta}{2}(v^n - 2u^{n-1} + u^{n-2}), \tag{2.8}$$

where the dimensionless parameter β is in the interval $(0, 1)$. In the limit of good time resolution, i.e., $\omega\triangle t \ll 1$, LF-hoRA2(3) provides higher-order accuracy for the amplitude and phase speed of the physical mode (see (2.13) and (2.14)).

Eliminating v^{n+1} in (2.7) and (2.8) gives

$$v^n = \frac{u^n - 2\beta u^{n-1} + \frac{\beta}{2}u^{n-2}}{1 - \frac{3}{2}\beta + i\beta\omega\triangle t},$$

and hence

$$v^{n+1} = \frac{u^{n+1} - 2\beta u^n + \frac{\beta}{2}u^{n-1}}{1 - \frac{3}{2}\beta + i\beta\omega\triangle t}.$$

Substituting v^n and v^{n+1} in (2.8) gives the equivalent formula of LF-hoRA2(3)

$$u^{n+1} - 2\beta u^n - (1 - 2\beta)u^{n-1} = i\omega\triangle t(2u^n - 3\beta u^{n-1} + \beta u^{n-2}). \tag{2.9}$$

Thus, the amplification factor, $A = u^{n+1}/u^n$, satisfies the following cubic equation.

$$A^3 - 2(\beta + i\omega\triangle t)A^2 + (3\beta i\omega\triangle t - 1 + 2\beta)A - \beta i\omega\triangle t = 0. \tag{2.10}$$

Equation (2.10) has three roots with one physical mode, denoted by A_+, and two computational modes. The exact solution to (2.3) is $u(t) = u(0)\exp(i\omega t)$ and the exact amplification factor is $A_{\text{exact}} = \exp(i\omega\triangle t)$.

The exact and the numerical amplification factors for LF-hoRA2(3) in the complex plane are plotted in Figure 2.1. The exact amplification factor lies on the unit circle as $\omega\triangle t$ increases from 0 to 1. Like the third-order Adams-Bashforth (AB3) method [10], the physical

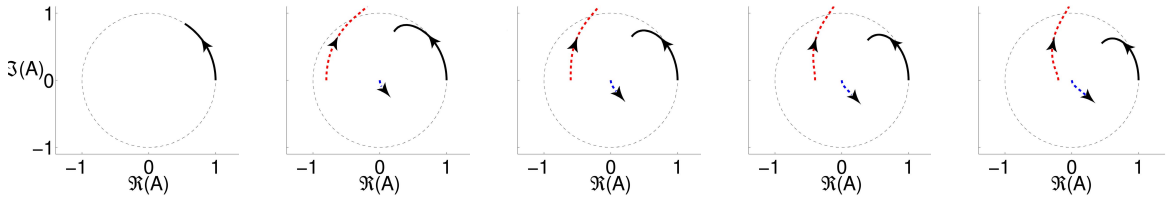

Figure 2.1: Amplification factors plotted in the complex plane. From left to right: exact amplification factor, amplification factors for LF-hoRA2(3) with $\beta = 0.1,\ 0.2,\ 0.3$ and 0.4, respectively. Solid line is the physical mode and two dashed curves represent computational modes.

mode of LF-hoRA2(3) stays inside the unit circle, while one computational mode becomes amplified when $\omega\triangle t$ exceeds $\sqrt{\frac{3}{4}+\beta-\beta^2}/(1+\frac{3}{2}\beta-\beta^2)$ (see (2.12) in Section 2.5).

Magnitudes of amplification factors for LF-hoRA2(3) are shown in Figure 2.2. Both computational modes are effectively controlled by the hoRA2(3) filter, especially when $\beta = 0.4$.

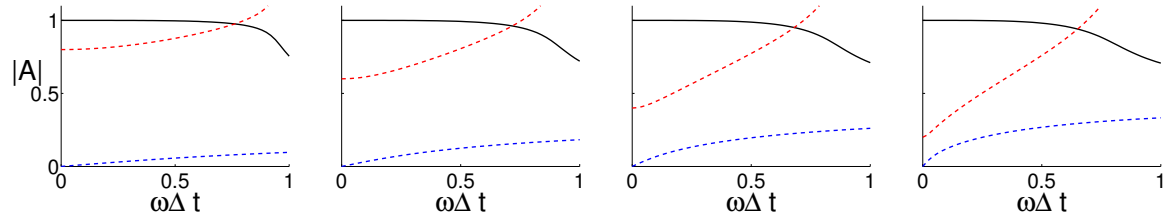

Figure 2.2: Magnitudes of amplification factors for LF-hoRA2(3), plotted as functions of $\omega\triangle t$. From left to right: $\beta = 0.1,\ 0.2,\ 0.3$ and 0.4, respectively. Solid line is the physical mode and two dashed curves represent computational modes.

2.4 CONSISTENCY ERROR

Applying the Taylor expansion to (2.9) gives the truncation error

$$\tau_n(\triangle t) = \frac{2-5\beta}{6}(i\omega\triangle t)^2 u'(t^n) + \frac{11\beta}{12}(i\omega\triangle t)^3 u'(t^n) + \mathcal{O}[(i\omega\triangle t)^4]. \tag{2.11}$$

This indicates that the scheme is second order in general, and achieves third-order overall accuracy when $\beta = 0.4$.

2.5 STABILITY

To determine the maximum $\omega\triangle t$ for which all numerical amplification factors are non-amplified, we follow the *root locus curve* method (see e.g., [15]). The characteristic equation of (2.9) is

$$\zeta^3 - 2\beta\zeta^2 - (1-2\beta)\zeta - z(2\zeta^2 - 3\beta\zeta + \beta) = 0,$$

where ζ denotes the points on the unit circle, i.e., $\zeta = e^{i\theta}$ for $\theta \in [0, 2\pi]$, and $z \in \mathbb{C}$. The curve formed by z is called the *root locus curve*. In our case $z = i\omega\triangle t$ lies on the imaginary axis, and consequently, we shall seek θ satisfying $\Re(z) = 0$. We find that

$$\cos\theta = 1 \text{ or } \cos\theta = \beta - \frac{1}{2},$$

which determines the following values of z:

$$z = 0 \text{ or } z = \pm i\frac{\sqrt{\frac{3}{4} + \beta - \beta^2}}{1 + \frac{3}{2}\beta - \beta^2}.$$

The above values are the intersection of the root locus curve with imaginary axis in the complex z-plane. Thus, the stability of the LF-hoRA2(3) scheme is provided by

$$\omega\triangle t \le \frac{\sqrt{\frac{3}{4} + \beta - \beta^2}}{1 + \frac{3}{2}\beta - \beta^2}, \quad 0 < \beta < 1. \tag{2.12}$$

Several root locus curves for various values of β are plotted in Figure 2.3.

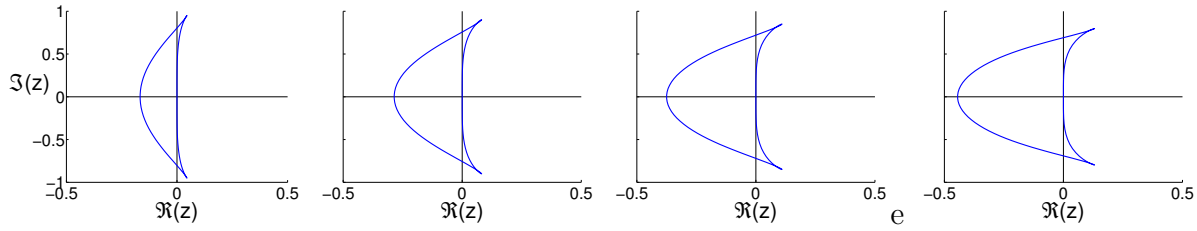

Figure 2.3: Root locus curves of LF-hoRA2(3). From left to right: $\beta = 0.1,\ 0.2,\ 0.3$ and 0.4, respectively. The stability of LF-hoRA2(3) is given by the intersection of the root locus curve with the imaginary axis.

2.6 ERROR ANALYSIS FOR AMPLITUDE AND PHASE SPEED

The first few terms in the Taylor expansion for the physical mode $A_+ = \sum_{n=0}^{\infty} a_n(\beta)(i\omega\triangle t)^n$ are[1]

$$a_0 = 1,\ a_1 = 1,\ a_2 = \frac{1}{2},\ a_3 = \frac{\beta}{4(1-\beta)},\ \text{and}\ a_4 = -\frac{1}{8} - \frac{\beta}{8(1-\beta)^2}.$$

The amplitude for the physical mode is fourth-order accurate in a single time step and hence is third-order accurate in a unit time:

$$|A_+| - |A_{\text{exact}}| = |A_+| - 1 = \frac{\beta(2\beta-3)}{8(1-\beta)^2}(\omega\triangle t)^4 + \mathcal{O}[(\omega\triangle t)^6],\ \beta \in (0,1). \tag{2.13}$$

Figure 2.4 compares magnitudes of the physical mode for various values of β. Note that the amplitude error grows as β increases.

The phase-speed error of the physical mode is

$$R_+ - 1 = \frac{\arg(A_+)}{\arg(A_{\text{exact}})} - 1 = \frac{2-5\beta}{12(1-\beta)}(\omega\triangle t)^2 + O[(\omega\triangle t)^4],\ \beta \in (0,1), \tag{2.14}$$

where $R_+ = \arg(A_+)/\arg(A_{\text{exact}})$ denotes the relative phase change in the physical mode. The phase speed of the physical mode is fourth-order accurate when $\beta = 0.4$ and second-order accurate otherwise. Figure 2.5 shows relative phase changes in the physical mode.

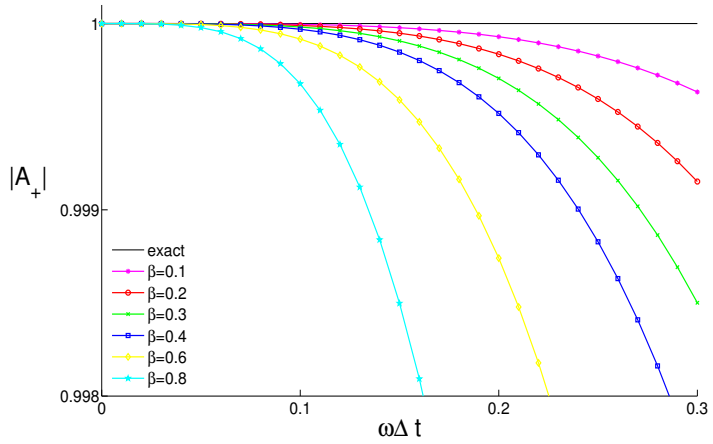

Figure 2.4: Magnitudes of the physical mode for LF-hoRA2(3) scheme, plotted as functions of $\omega\triangle t$.

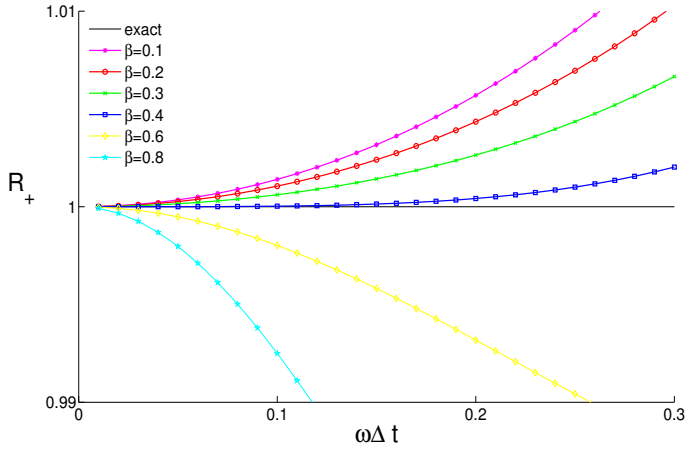

Figure 2.5: Relative phase changes in the physical mode for LF-hoRA2(3), plotted as functions of $\omega\triangle t$.

The phase-speed error decays as β increases from 0 to 0.4, and then grows as β increases afterwards.

[1]The coefficients of the Taylor expansion are obtained using symbolic manipulation of Mathematica.

Table 2.1 summarizes several properties of the amplitude and phase-speed errors for the physical mode of LF-hoRA2(3). Since both amplitude and phase-speed errors increase when $\beta > 0.4$, we narrow down the choice of β within the interval $(0, 0.4]$.

	$\beta \in (0, 0.4]$	$\beta \in (0.4, 1)$	Order of accuracy
Amplitude error	$\nearrow$	$\nearrow$	3rd
Phase-speed error	$\searrow$	$\nearrow$	4th at $\beta = 0.4$, 2nd otherwise

Table 2.1: Changes in amplitude and phase-speed errors for the physical mode of LF-hoRA2(3) as β varies. The notation $\nearrow$ and $\searrow$ indicate the increase and decrease in the errors as β grows, respectively.

2.7 COMPARISON OF RA, RAW AND HORA FILTERS

In Figure 2.6, we compare magnitudes of the physical modes for LF-RA, LF-RAW and LF-hoRA3. In order to have the same damping rate of the most unstable computational mode of each scheme, we choose the RA-parameter $\nu = 0.8$, RAW-parameters $\alpha = 0.53$, $\nu = 0.8$ and the hoRA3-parameter $\beta = 0.4$.[2] The amplitudes of the physical modes for LF-RA and LF-RAW become amplified when $\omega\triangle t$ exceeds 0.66 and 0.35, respectively. While the amplitude of the physical mode for LF-hoRA3 stays below unity, one of the computational modes becomes amplified when $\omega\triangle t > 0.69$, as seen in Figure 2.2. The amplitude of LF-hoRA3 is third order, while the amplitudes of both LF-RA and LF-RAW are only first order (see Table 2.2).

Figure 2.7 compares the relative phase changes in the physical modes. The phase-speed error of the LF-hoRA3 is significantly smaller than the phase-speed errors of both LF-RA and LF-RAW within the stability region.

[2] In the limit of good time resolution ($\omega\triangle t \ll 1$), the damping rates of the computational mode in LF-RA and LF-RAW are $1 - \nu$, while the damping rate of the most unstable computational mode in LF-hoRA2(3) is $1 - 2\beta$.

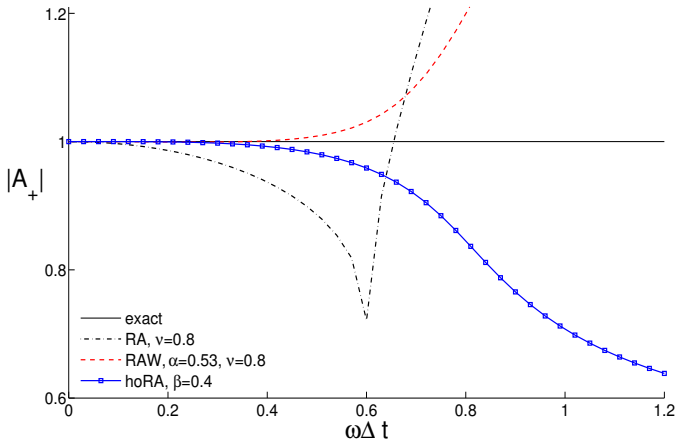

Figure 2.6: Magnitudes of the physical modes, plotted as functions of $\omega\triangle t$.

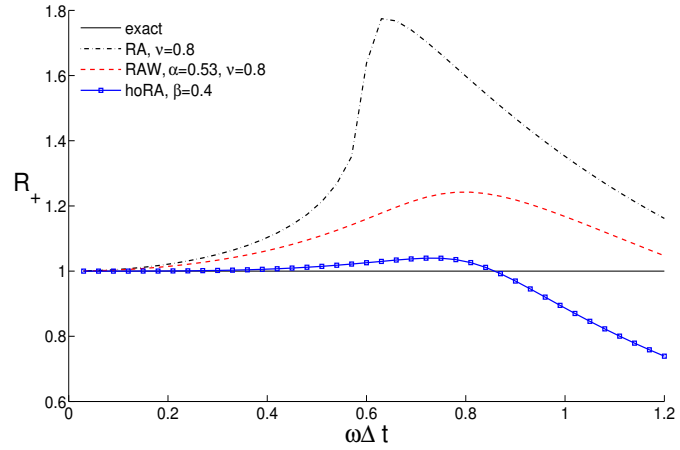

Figure 2.7: Relative phase changes in the physical modes, plotted as functions of $\omega\triangle t$.

2.8 COMPARISON OF LF-HORA3 AND AB3 SCHEMES

The third-order LF-hoRA3 has the following properties:

(i) it follows from (2.11) that the truncation error is

$$\tau_n(\triangle t) = \frac{11}{30}(i\omega\triangle t)^3 u'(t^n) + \mathcal{O}[(i\omega\triangle t)^4],$$

(ii) by (2.12), it is stable for $\omega\triangle t \leq 0.69$,

(iii) it requires one new function evaluation per time step.

Recall that the *efficiency factor* is defined as the maximum stable time step with which the oscillation equation can be integrated, divided by the number of function evaluations per time step [10]. It follows from (ii) and (iii) that the efficiency factor of LF-hoRA3 is 0.69.

On the other hand, the AB3 method reads

$$u^{n+1} = u^n + \frac{\triangle t}{12}\left(23F(u^n) - 16F(u^{n-1}) + 5F(u^{n-2})\right),$$

has the following properties [10]:

(i) the truncation error is

$$\tau_n(\triangle t) = \frac{3}{8}(i\omega\triangle t)^3 u'(t^n) + \mathcal{O}[(i\omega\triangle t)^4],$$

(ii) the method is stable for $\omega\triangle t \leq 0.72$,

(iii) it also requires one new function evaluation in each time step.

The efficiency factor of AB3 method is 0.72. Thus, the LF-hoRA3 is almost as accurate, stable and efficient as the intrusive AB3 method.

As in [10], Table 2.2 summarizes several properties of the aforementioned time-stepping methods.

2.9 NUMERICAL TESTS

In this section we perform several numerical tests on the leapfrog scheme combined with RA, RAW and hoRA3, and on the AB3 method. As in Section 2.7, we choose the filter parameters such that the damping rate of the most unstable computational mode of each scheme is the same. Section 2.9.1 and Section 2.9.2 show that the hoRA filter preserves both amplitude and phase with high accuracy. Section 2.9.3 shows that the LF-hoRA3 scheme captures the physics of a model with reasonable fidelity.

Method	Order	Strg. factor	Amplitude	Phase speed	Max. $\omega\triangle t$
Leapfrog	2	2	1	$1+\frac{(\omega\triangle t)^2}{6}$	1
LF-RA	1	3	$1-\frac{\nu}{2(2-\nu)}(\omega\triangle t)^2$	$1+\frac{1+\nu}{3(2-\nu)}(\omega\triangle t)^2$	$\sqrt{\frac{2-\nu}{2+\nu}}$
LF-RAW	1	4	$1+\frac{\nu(1-2\alpha)}{2(2-\nu)}(\omega\triangle t)^2$	$1+\left(\frac{(1-\nu(1-\alpha))(2-\alpha\nu)}{(2-\nu)^2}-\frac{1}{3}\right)(\omega\triangle t)^2$	$\mu(\alpha,\nu)$
LF-hoRA2	2	4	$1+\frac{\beta(2\beta-3)}{8(1-\beta)^2}(\omega\triangle t)^4$	$1+\frac{2-5\beta}{12(1-\beta)}(\omega\triangle t)^2$	$\frac{\sqrt{\frac{3}{4}+\beta-\beta^2}}{1+\frac{3}{2}\beta-\beta^2}$
LF-hoRA3	3	4	$1-0.306(\omega\triangle t)^4$	$1+0.024(\omega\triangle t)^4$	0.69
AB3	3	4	$1-0.375(\omega\triangle t)^4$	$1+0.401(\omega\triangle t)^4$	0.72

Table 2.2: Comparison of time-stepping schemes. The explicit form of $\mu(\alpha,\nu)$ is given by $\mu(\alpha,\nu)=\sqrt{\frac{(2\alpha-1)(2-\nu)}{\alpha^2(2+\nu(2\alpha-1))}}$ [20].

2.9.1 Simple pendulum

Consider a simple pendulum problem, which is given by two coupled nonlinear equations (also see [50]):

$$\begin{aligned}\frac{d\theta}{dt} &= v/L,\\ \frac{dv}{dt} &= -g\sin\theta,\end{aligned}$$

where θ, v, L and g denote, respectively, angular displacement, velocity along the arc, length of the pendulum, and the acceleration due to gravity. Set $g=9.8$ and $L=49$ to easily observe the long time behavior of the numerical solutions. We choose the initial condition $(\theta_0,v_0)=(0.9\pi,0)$ at $t=0$ and the time step $\triangle t=0.1$, and then numerically integrate the system using LF-RA ($\nu=0.8$), LF-RAW ($\alpha=0.53$, $\nu=0.8$) and LF-hoRA3 over the time interval $[0,200]$. The Runge-Kutta (RK) 4 method is used to initialize the second step of each scheme and also for the third step of LF-hoRA3. Then compare the corresponding results with the reference solution, which is computed using the adaptive RK4(5) method with relative error tolerance 10^{-10} and absolute error tolerance 10^{-15}.

The comparison is shown in Figure 2.8. The RA filter damps the amplitude quickly while the RAW filter damps the amplitude slowly. The phase errors of both LF-RA and LF-RAW

solutions are relatively large. The hoRA3 filter preserves the amplitude and phase with high accuracy even after a long time period.

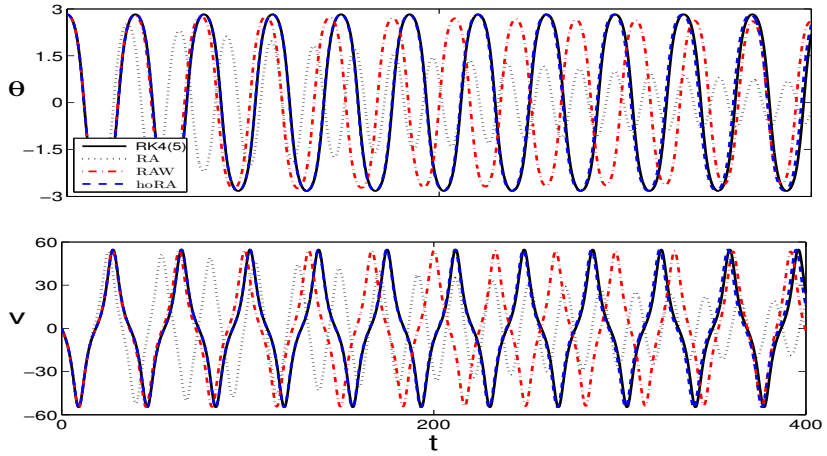

Figure 2.8: Numerical solutions to the simple pendulum, computed by LF-RA ($\nu = 0.8$), LF-RAW ($\alpha = 0.53$, $\nu = 0.8$) and LF-hoRA3 ($\beta = 0.4$), are compared with the reference solutions obtained from adaptive RK4(5) method with relative error tolerance 10^{-10} and absolute error tolerance 10^{-15}. The initial condition is $(\theta_0, v_0) = (0.9\pi, 0)$ at $t = 0$ and the time step is $\triangle t = 0.1$.

2.9.2 Lorenz system

Consider the Lorenz system

$$\begin{aligned} \frac{dX}{dt} &= \sigma(Y - X), \\ \frac{dY}{dt} &= -XZ + rX - Y, \\ \frac{dZ}{dt} &= XY - bZ. \end{aligned}$$

As in [10], we choose $\sigma = 12$, $r = 12$, $b = 6$, and the initial condition $(X_0, Y_0, Z_0) = (-10, -10, 25)$ at $t = 0$. The system is numerically integrated over the time interval $[0, 2.5]$ using LF-RA, LF-RAW, LF-hoRA3 and AB3 methods, with time step $\triangle t = 0.025$ and all

other filter-parameters exactly the same as in the previous test. Again, the reference solution is computed using the adaptive RK4(5) method with the same error tolerances as before.

The numerical solutions for X are plotted in Figure 2.9 (the reference solution is almost overlapped by LF-hoRA3 solution). As predicted by the linear analysis, the LF-hoRA3 is almost as accurate as the AB3 method.

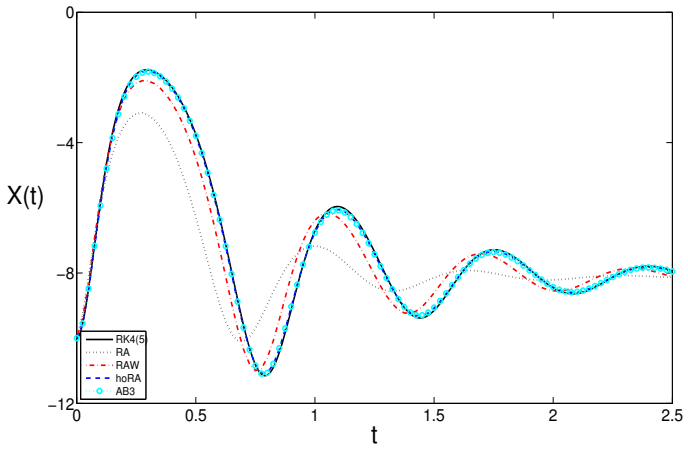

Figure 2.9: Numerical solutions to Lorenz system for variable X, computed by LF-RA ($\nu = 0.8$), LF-RAW ($\alpha = 0.53$, $\nu = 0.8$), LF-hoRA3 ($\beta = 0.4$) and AB3, are compared with the reference solution obtained from the adaptive RK4(5) method with relative error tolerance 10^{-10} and absolute error tolerance 10^{-15}. The initial condition is $(X_0, Y_0, Z_0) = (-10, -10, 25)$ at $t = 0$ and the time step is $\triangle t = 0.025$.

2.9.3 Ozone photochemistry

Consider an example of reactions between atomic oxygen (O), nitrogen oxides (NO and NO_2), and ozone (O_3) (see [11] for more details):

$$\begin{aligned} NO_2 + h\nu &\xrightarrow{k_1} NO + O, \\ O + O_2 &\xrightarrow{k_2} O_3, \\ NO + O_3 &\xrightarrow{k_3} O_2 + NO_2, \end{aligned}$$

where $h\nu$ denotes a photon of solar radiation. Let $c = (c_1, c_2, c_3, c_4)$ represent the concentration in molecules per cubic centimeter of O, NO, NO_2 and O_3, respectively. Assuming that the background concentration of O_2 is constant, the reactions are governed by the following system:

$$\begin{aligned}
\frac{dc_1}{dt} &= k_1 c_3 - k_2 c_1, \\
\frac{dc_2}{dt} &= k_1 c_3 - k_3 c_2 c_4, \\
\frac{dc_3}{dt} &= k_3 c_2 c_4 - k_1 c_3, \\
\frac{dc_4}{dt} &= k_2 c_1 - k_3 c_2 c_4.
\end{aligned}$$

Here

$$k_1 = 10^{-2} \max\{0, \sin(2\pi t/t_d)\} \mathrm{s}^{-1},$$

$$k_2 = 10^{-2} \mathrm{s}^{-1},^{3}\ k_3 = 10^{-16} \mathrm{cm}^3 \mathrm{molecule}^{-1} \mathrm{s}^{-1},$$

where t_d is the length of 1 day in seconds. With initial condition $c_0 = (0, 0, 5 \times 10^{11}, 8 \times 10^{11})$ molecules cm^{-3} at $t = 0$, the reference solution is computed using the adaptive RK4(5) method with same error tolerances as before, and the numerical solution is computed using LF-hoRA3 and time step $\triangle t = 40$ s. The chemical concentrations over the next 2 days are shown in Figure 2.10. With the fixed time step, the LF-hoRA3 is able to capture the behavior of the concentrations with reasonable accuracy.

2.10 CONCLUSIONS

In this chapter we proposed and analyzed a higher-order Robert-Asselin type time filter, hoRA2(3). It is an efficient and non-intrusive post process to the LF scheme and easily implementable in existing legacy codes. Moreover, with the same computational effort and storage requirement as RAW filter, the proposed filter increases the numerical accuracy to third order. Thus, the LF-hoRA2(3) is suitable to simulate the long-time behavior of weather and climate models.

[3] We choose $k_2 = 10^{-2}$ instead of 10^5 as in [11], to make the reaction equations non-stiff.

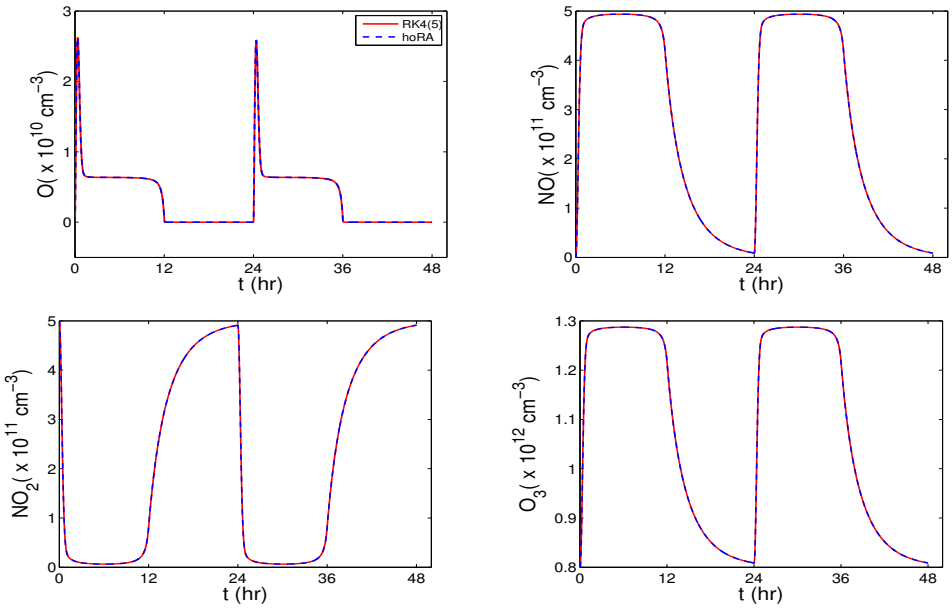

Figure 2.10: Numerical solutions for chemical concentrations, computed using LF-hoRA3, are compared with the reference solutions obtained from adaptive RK4(5) method with relative error tolerance 10^{-10} and absolute error tolerance 10^{-15}. The initial condition is $c_0 = (0, 0, 5 \times 10^{11}, 8 \times 10^{11})$ molecules cm^{-3} at $t = 0$, and the time step is $\triangle t = 40$ s.

3.0 THE BEHAVIOR OF HIGHER-ORDER ROBERT–ASSELIN TIME FILTER IN THE IMPLICIT-EXPLICIT SCHEME

3.1 INTRODUCTION

The atmosphere and ocean support several types of waves that propagate at very different speeds. If an explicit time differencing is used to approximate the time derivative in the equations governing a system, the maximum stable time step will be limited by the speed of the most rapidly propagating waves (e.g., sound waves and gravity-inertia waves). Early numerical weather prediction models used the explicit LF scheme, and the maximum permissible time step has to be small enough for the integration to be stable.

In order to relieve the severe time step restriction, it is common to treat the high-frequency waves implicitly and the remaining terms explicitly (e.g., [12, 22, 47, 49]). This implicit-explicit (IMEX) numerical technique was pioneered by Robert in 1969 [41]. In contrast to a fully explicit scheme, the IMEX scheme eliminates the time step restriction imposed by the high-frequency modes. In atmospheric sciences, the Crank-Nicolson-Leapfrog (CNLF) method is widely used (e.g., [24]), which treats the rapidly-moving waves implicitly using the Crank-Nicolson scheme to stabilize the fast-moving waves, while the remaining slower-moving waves are treated by the explicit leapfrog scheme.

Similar to the previous chapter, we consider the hoRA2(3)-filtered CNLF scheme (hereafter, CNLF-hoRA for notational simplicity). For a generic tendency equation

$$\frac{\partial u}{\partial t} = L(u) + F(u), \tag{3.1}$$

the CNLF-hoRA reads

$$\frac{u^{n+1} - \overline{u^{n-1}}}{2\triangle t} = \left(\frac{1}{2}L\left(u^{n+1}\right) + \frac{1}{2}L\left(\overline{u^{n-1}}\right)\right) + F(u^n),$$

$$\overline{u^n} = u^n + \frac{\beta}{2}\left(u^{n+1} - 2u^n + \overline{u^{n-1}}\right) - \frac{\beta}{2}\left(u^n - 2\overline{u^{n-1}} + \overline{u^{n-2}}\right).$$

Here L is a linear operator that includes the high-frequency wave propagation, and F is a nonlinear operator that includes low-frequency wave propagation representing advection and other processes.[1] In this chapter, we give a complete stability and error analysis of CNLF-hoRA. The method is then implemented in the elastic pendulum [33, 49] and the acoustic advection problem [42] to verify the theoretical results. The work of this chapter is based on [29].

3.2 THE CNLF-HORA SCHEME

Analogous to the previous chapter, an IMEX method for non-dissipative dynamical systems may be examined by analyzing solutions to the oscillation equation

$$\frac{du}{dt} = i\omega_H u + i\omega_L u, \tag{3.2}$$

where ω_H and ω_L are frequencies of fast and slow waves, corresponding to $L(u)$ and $F(u)$ in (3.1), respectively.

The CNLF-hoRA discretizes, respectively, the ω_H term using CN and the ω_L term with the LF, and the filter follows to update the provisional variables:

$$\frac{v^{n+1} - u^{n-1}}{2\triangle t} = i\omega_H\left(\frac{v^{n+1} + u^{n-1}}{2}\right) + i\omega_L v^n, \tag{3.3}$$

$$u^n = v^n + \frac{\beta}{2}(v^{n+1} - 2v^n + u^{n-1}) - \frac{\beta}{2}(v^n - 2u^{n-1} + u^{n-2}), \tag{3.4}$$

where the dimensionless parameter $\beta \in (0, 0.4]$. Eliminating v^{n+1} in (3.3) and (3.4) gives

$$v^n = \frac{(1 - i\omega_H\triangle t)u^n - \beta(2 - i\omega_H\triangle t)u^{n-1} + \frac{\beta}{2}(1 - i\omega_H\triangle t)u^{n-2}}{\left(1 - \frac{3}{2}\beta\right)(1 - i\omega_H\triangle t) + i\beta\omega_L\triangle t},$$

[1] If the terms representing high-frequency waves are nonlinear, they may be linearized to form L, and the remaining nonlinear contributions may be incorporated in F.

and therefore

$$v^{n+1} = \frac{(1 - i\omega_H \triangle t)u^{n+1} - \beta(2 - i\omega_H \triangle t)u^n + \frac{\beta}{2}(1 - i\omega_H \triangle t)u^{n-1}}{\left(1 - \frac{3}{2}\beta\right)(1 - i\omega_H \triangle t) + i\beta\omega_L \triangle t}.$$

Substituting v^n and v^{n+1} into (3.4) gives the equivalent multistep method of CNLF-hoRA

$$\begin{aligned} u^{n+1} - 2\beta u^n - (1 - 2\beta)u^{n-1} = & i\omega_H \triangle t(u^{n+1} - \beta u^n + (1 - \beta)u^{n-1}) \\ & + i\omega_L \triangle t(2u^n - 3\beta u^{n-1} + \beta u^{n-2}). \end{aligned} \tag{3.5}$$

It is easy to check that the CNLF-hoRA recovers the explicit LF-hoRA2(3) (2.7)-(2.8) when $\omega_H = 0$, i.e., when the waves are not split.

3.3 ERROR ANALYSIS FOR AMPLITUDE AND PHASE SPEED

The amplification factor, $A = u^{n+1}/u^n$, of (3.5) satisfies the following cubic equation.

$$aA^3 + bA^2 + cA + d = 0, \tag{3.6}$$

where

$$\begin{aligned} a &= 1 - i\omega_H \triangle t, & b &= -2\beta - 2i\omega_L \triangle t + \beta i\omega_H \triangle t, \\ c &= -1 + 2\beta - (1 - \beta)i\omega_H \triangle t + 3\beta i\omega_L \triangle t, & d &= -\beta i\omega_L \triangle t. \end{aligned}$$

Equation (3.6) has three roots with one physical mode, denoted by A_+, and two computational modes. Let $r = \omega_H/\omega_L$, then the exact solution to (3.2) is

$$u(t) = u(0)\exp(i\omega_H t + i\omega_L t) = u(0)\exp(i(1 + r)\omega_L t),$$

and the exact amplification factor is

$$A_{\text{exact}} = \exp(i(1 + r)\omega_L \triangle t).$$

The Taylor expansion of the physical mode is $A_+ = \sum_{n=0}^{\infty} a_n (i\omega_L \triangle t)^n$, where the first few are given by[2]

$$a_0 = 1,\ a_1 = 1 + r,\ a_2 = (1+r)^2/2,\ a_3 = (1+r)^2 \left(\frac{\beta + (2-\beta)r}{4(1-\beta)} \right),$$
$$a_4 = (1+r)^3 \left(\frac{(2-4\beta)r - (1-r)(\beta + (1-\beta)^2)}{8(1-\beta)^2} \right).$$

The amplitude of the physical mode is fourth-order accurate per time step, and thus is third-order accurate per unit time:

$$|A_+| = 1 + (1+r)^3 \frac{\beta(2\beta - 3 - r)}{8(1-\beta)^2} (\omega_L \triangle t)^4 + \mathcal{O}((\omega_L \triangle t)^6).$$

The phase speed of the physical mode is

$$R_+ = \frac{\arg(A_+)}{\arg(A_{\text{exact}})} = 1 + \frac{(1+r)}{12(1-\beta)} \left(2 - 5\beta - (4-\beta)r\right) (\omega_L \triangle t)^2 + \mathcal{O}((\omega_L \triangle t)^4).$$

Notice that because of the presence of CN discretization, the phase speed is only second-order accurate. Indeed, the overall accuracy of CNLF-hoRA is second order for every $\beta \in (0, 0.4]$.

3.4 STABILITY

The magnitudes of the amplification factor $|A|$ for CNLF-hoRA are contoured as a function of $\omega_L \triangle t$ and $\omega_H \triangle t$ in Figure 3.1. Since $|A|$ in the lower-half plane is antisymmetric about the origin, only the upper-half plane is plotted. In the absence of ω_H, the time step condition is given by (2.12)

$$\mu_{\text{hoRA}} = \frac{\sqrt{4 - (2\beta - 1)^2}}{(2-\beta)(2\beta + 1)}.$$

In the presence of ω_H, the stability ($|\omega_L \triangle t| < \mu_{\text{hoRA}}$) possesses a weak instability when ω_L and ω_H are of opposite sign (light gray region). Thus, CNLF-hoRA is stable when $|\omega_L \triangle t| < \mu_{\text{hoRA}}$, as well as the ratio $r = \omega_H/\omega_L$ is bigger than a threshold, $r_0(\beta)$, which depends on the filter parameter β. We found empirically that the threshold is bounded above

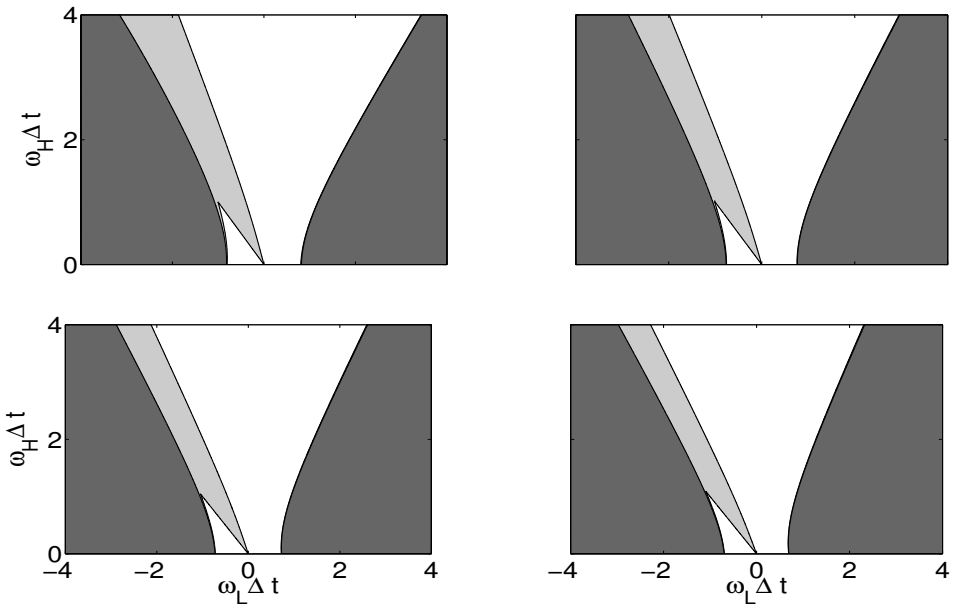

Figure 3.1: Magnitudes of the amplification factor of CNLF-hoRA for $\beta = 0.1$ (left-top), $\beta = 0.2$ (right-top), $\beta = 0.3$ (left-bottom) and $\beta = 0.4$ (right-bottom). Regions with $1 < |A| < 1.01$ are shaded with light gray and regions in which $|A| > 1.01$ are shaded with dark gray. Only the upper-half plane is plotted since $|A|$ in the lower-half plane is antisymmetric about the origin.

by 2.25, and is decreasing as β grows. For β=0.1, 0.2, 0.3 and 0.4, the values of $r_0(\beta)$ are 2.13, 2.08,1.89 and 1.78, respectively.

As in [12], we use two parameters, μ and r_0, to describe the stability region of a general IMEX scheme, where μ is the maximum $\omega\triangle t$ of the corresponding fully explicit scheme, and r_0 is the smallest value for which the numerical solution is stable regardless of the value $\triangle t$, provided $\omega_H > r_0\omega_L$. The CNLF scheme with the Robert–Asselin–Williams filter (CNLF-RAW) [49] is unconditionally stable when $r \geq r_0 \approx 1$, thus the wedge-shaped stability region is wider than the region of CNLF-hoRA. However, there is a reduction in stability when $\omega_H\triangle t$ is small. For example, $\mu = 0.44$ for filter parameters $\nu = 0.2, \alpha = 0.53$, and $\mu = 0$ for $\nu = 0.2, \alpha = 0.5$. Durran and Blossey [12] proposed several IMEX schemes:

[2]The coefficients of the Taylor expansion are obtained using symbolic manipulation of Mathematica 9.0.0.

AM2*AX2*, AI2*AB3, BI2*BX3* and BDF2BX2*. The explicit stability μ for these schemes in the absence of $\omega_H \triangle t$ are $\mu = 0.76, 0.72, 0.67$ and 0.72, which are comparable with value of CNLF-hoRA $\mu = 0.69$. In the presence of $\omega_H \triangle t$, the wedge-shaped stability region of AI2*AB3 ($r_0 = 1.23$) is wider than the region of CNLF-hoRA, while the regions of the other three schemes are narrower ($r_0 = 3, 2.43$ and 5 for AM2*AX2*, BI2*BX3* and BDF2BX2*, respectively). The values of μ and r_0 for these methods are listed in Table 3.1.

Implicit	Explicit	μ	r_0
AM2*	AX2*	0.76	3
AI2*	AB3	0.72	1.23
BDF2	BX2*	0.67	5
BI2*	BX3*	0.72	2.43
CN	LF-RAW ($\nu = 0.2, \alpha = 0.53$)	0.44	1
CN	LF-RAW ($\nu = 0.2, \alpha = 0.5$)	0	1
CN	LF-hoRA2(3)	μ_{hoRA}	< 2.25

Table 3.1: Parameters μ and r_0 which characterize the stability regions for various IMEX schemes.

3.5 STABILITY TEST FOR LINEARIZED SHALLOW-WATER EQUATIONS

The shallow-water equations are often used in numerical weather prediction to test new numerical methods. The linearized equations possess two kinds of associated motion, high-frequency gravitational oscillations and low-frequency Rossby modes. The speed of gravity mode is six times faster than that associated with the Rossby modes that govern the weather [44], and this leads to time steps that are six times shorter than those associated with an explicit treatment of advection (Rossby modes).

Denote $\vec{\varphi} = \left(u, v, \frac{\phi}{c}\right)^T$, where u and v are the velocity components in the x- and y-directions respectively, ϕ is the perturbation geopotential, $c = \sqrt{gH}$ and H is the reference depth. The shallow-water equations, linearized in one dimension about a constant zonal flow on the f-plane, are given by (see e.g., [22])

$$\frac{\partial \vec{\varphi}}{\partial t} = \begin{pmatrix} -\overline{u}\frac{\partial}{\partial x} & f & -c\frac{\partial}{\partial x} \\ -f & -\overline{u}\frac{\partial}{\partial x} & 0 \\ -c\frac{\partial}{\partial x} & 0 & -\overline{u}\frac{\partial}{\partial x} \end{pmatrix} \vec{\varphi}.$$

Assuming that the solution φ is in the form $\varphi(x,t) = \Psi(t)e^{ikx}$, the above equation can be written as follows:

$$\frac{d\Psi}{dt} = L\Psi + F\Psi, \tag{3.7}$$

where

$$L = \begin{pmatrix} 0 & 0 & -ikc \\ 0 & 0 & 0 \\ -ikc & 0 & 0 \end{pmatrix} \quad \text{and} \quad F = \begin{pmatrix} -ik\overline{u} & f & 0 \\ -f & -ik\overline{u} & 0 \\ 0 & 0 & -ik\overline{u} \end{pmatrix}.$$

The terms kc and $k\overline{u}$ are identified as the high and low frequencies, respectively. Thus, we will treat L implicitly, and F explicitly. Integrating (3.7) using CNLF-hoRA, the discretized system becomes

$$P_3\Psi^{n+1} + P_2\Psi^n + P_1\Psi^{n-1} + P_0\Psi^{n-2} = 0, \tag{3.8}$$

where each P_n is a 4×4 matrix, with

$$P_3 = I - \triangle t L, \qquad P_2 = -2\beta I + \triangle t\beta L - 2\triangle t F,$$
$$P_1 = (-1 + 2\beta)I - \triangle t(1-\beta)L + 3\triangle t\beta F, \qquad P_0 = -\triangle t\beta F.$$

The associated eigenvalue problem of (3.8) is

$$\left(\lambda^3 P_3 + \lambda^2 P_2 + \lambda P_1 + P_0\right)\Psi^{n-2} = 0.$$

For $f = 0$, the maximum modulus of the eigenvalue for various values of β are plotted as a function of $\omega_L \triangle t$ and $\omega_H \triangle t$, in Figure 3.2. As analyzed in Section 3.4, the CNLF-hoRA scheme is stable when $\omega_L \triangle t < \mu_{\text{hoRA}}$ and $\omega_H > r_0 \omega_L$, and also for $\omega_H < \omega_L$. The CNLF-RAW ($\alpha = 0.5, \nu = 0.2$) is unstable (not shown). This is due to the instability in the explicit integration. The situation is improved when $\alpha = 0.53$ (not shown), in which case the scheme is stable under the conditions $\omega_H > \omega_L$ and $\omega_L \triangle t < 0.44$. If we take $f = 10^{-3}$, the stability regions are almost unchanged (not shown).

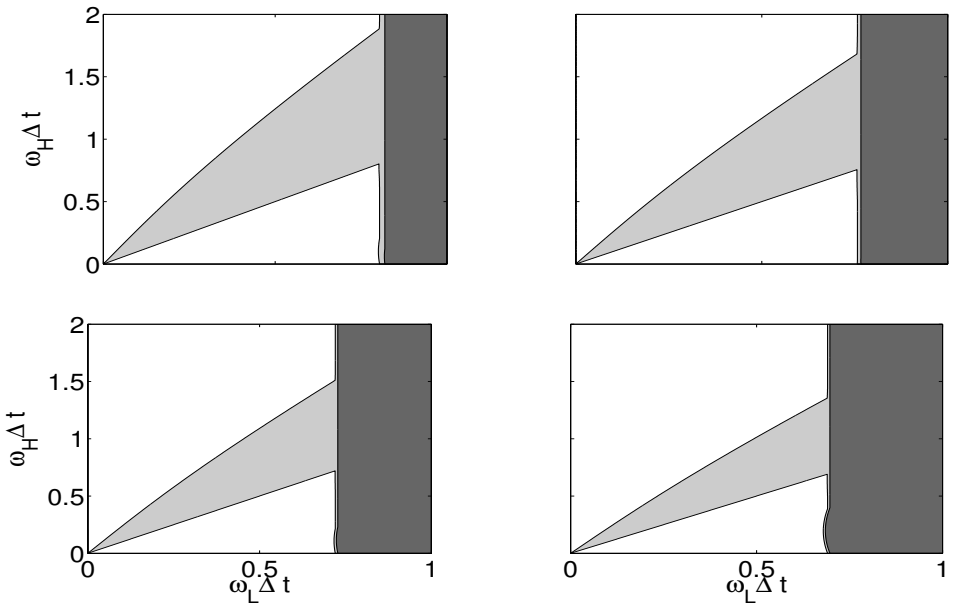

Figure 3.2: Magnitudes of the amplification factor (defined as the modulus of the largest eigenvalue of the propagator matrix) of CNLF-hoRA applied to linearized shallow-water equations (3.7) for $\beta = 0.1$ (left-top), $\beta = 0.2$ (right-top), $\beta = 0.3$ (left-bottom) and $\beta = 0.4$ (right-bottom). Regions with $1 < |A| < 1.01$ are shaded with light gray and regions in which $|A| > 1.01$ are shaded with dark gray. Only the upper-right quadrant is plotted as the value of $|A|$ is symmetric about the origin.

3.6 NUMERICAL TESTS

3.6.1 Elastic pendulum

In this section, we test several IMEX schemes on an elastic pendulum problem [33]. The elastic pendulum is governed by four coupled nonlinear ordinary differential equations in polar coordinates:

$$\begin{aligned} r' &= p_r/m, \\ p_r' &= p_\theta^2/mr^3 - k(r-\ell_0) + mg\cos\theta, \\ \theta' &= p_\theta/mr^2, \\ p_\theta' &= -mgr\sin\theta, \end{aligned}$$

where g is the gravitational acceleration, ℓ_0 is the unstretched length of the spring, k is its stiffness, m is the mass of the bob, r is the length of the spring, θ is the angular displacement, p_r and p_θ are the radial and angular momenta, respectively. The mechanical system has two motions, namely the rotational oscillations and the elastic oscillations. The rotational oscillations are similar to the simple (anelastic) pendulum, and the corresponding frequency is $\omega_L = \sqrt{g/\ell}$, where ℓ is the length of the loaded spring at equilibrium state. The elastic oscillations, on the other hand, are due to the elastic spring that the bob oscillates back and forth, and the corresponding frequency is $\omega_H = \sqrt{k/m}$. The rotational motions are considered to correspond to the rotational or Rossby-Haurwitz waves, while the elastic motions are analogues of the high frequency gravity waves in the atmosphere.

By letting $r = \ell(1+\eta)$, the above governing equations can be written in terms of ω_L and ω_H, which are given as follows (see [49]).

$$\eta' = \underline{\nu_\eta}, \tag{3.9}$$

$$\nu_\eta' = -\omega_L^2(1-\cos\theta) - \underline{\omega_H^2\eta} + (1+\eta)\nu_\theta^2, \tag{3.10}$$

$$\theta' = \nu_\theta, \tag{3.11}$$

$$\nu_\theta' = \left(-\omega_L^2\sin\theta - 2\nu_\eta\nu_\theta\right)/(1+\eta). \tag{3.12}$$

The underlined terms in (3.9) and (3.10) are related to the high frequency elastic oscillations, and thus they impose restrictive time step condition if they are integrated explicitly. Therefore, we will treat the underlined terms implicitly and all the other terms explicitly.

We take $\omega_L = 3$ and $\omega_H = 30$, and numerically integrate (3.9)–(3.12) for the time interval $[0, 50]$ with several IMEX schemes. These numerical solutions are compared with the reference solution, which is computed using the explicit fourth-order Runge-Kutta method (RK4) with time step $\triangle t = 10^{-6}$. In general, the permissible time step is smaller than that provided in the linear analysis because of the nonlinearity, (see e.g., [32]). We found that in the present test, the maximum stable time step of each IMEX scheme is 5-6 times larger than that of the corresponding fully explicit scheme.

The accuracy of these IMEX methods is compared in Figure 3.3, which shows the relative error in θ plotted on a log-log scale as a function of $\omega_L \triangle t$. The relative error is evaluated as the normalized difference between the numerical and reference solutions of θ at $T = 50$. Except CNLF-RAW ($\alpha = 0.53$, $\nu = 0.2$), all other schemes converge quadratically, as expected. All second-order schemes behave similarly for small time steps, but CNLF-hoRA with $\beta = 0.1$ is slightly more accurate for larger step sizes.

3.6.2 Acoustic advection

In this section, we consider a one-dimensional acoustic advection problem on a periodic domain $[0, 1]$ (see [42])

$$u_t + U u_x + c_s p_x = 0, \tag{3.13}$$

$$p_t + U p_x + c_s u_x = 0, \tag{3.14}$$

with a sound velocity c_s that is significantly faster than the advection velocity U. We split the equations so that the advection is treated explicitly while acoustic waves are integrated implicitly. The initial data is set $u(x, 0) = 0$ and $p(x, 0) = p_0(x) = \sin(2\pi x) + \sin(5\pi x)$, and the analytical solutions are

$$u(x,t) = 0.5p_0\left(x - (U + c_s)t\right) - 0.5p_0\left(x - (U - c_s)t\right),$$

$$p(x,t) = 0.5p_0\left(x - (U + c_s)t\right) + 0.5p_0\left(x - (U - c_s)t\right).$$

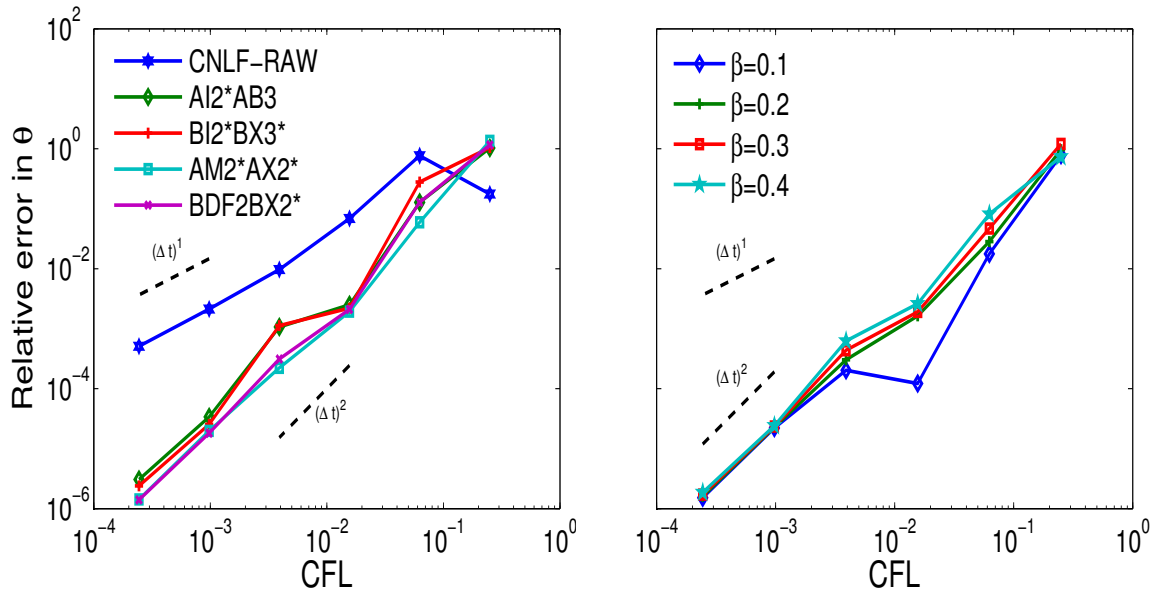

Figure 3.3: Log-log plot of the relative error in the angular displacement (θ) for $\omega_L = 3$ and $\omega_H = 30$, as a function of $\omega_L \triangle t$ for several IMEX schemes. The filter parameters of CNLF-RAW are $\alpha = 0.53$ and $\nu = 0.2$. The right-hand side figure is for CNLF-hoRA with various values of the filter parameter.

We set $T = 1.5$, $U = 0.1$ and $c_s = 1.0$. The relative error of the advection velocity in the $\|\cdot\|_{L^2}$ norm is evaluated at the final time. All runs use 500 nodes in the space domain. Table 3.2-3.3 summarize the relative errors for several IMEX methods. As expected, CNLF-RAW is first-order convergent and all other methods exhibit second-order convergence. As in the previous test, CNLF-hoRA with smaller value of β is more accurate than that with larger value of β.

3.7 CONCLUSIONS

In this chapter we performed error and stability analysis for the CNLF-hoRA method. Unlike LF-hoRA2(3), the IMEX scheme is second-order accurate for all filter parameter values

# of time steps	AI2*AB3	AM2*AX2*	BDF2BX2*	BI2*BX3*	CNLF-RAW
320	2.163e-2	6.560e-3	6.872e-3	1.784e-2	9.178e-3
640	5.168e-3	1.602e-3	1.619e-3	4.170e-3	3.201e-3
1280	1.293e-4	4.013e-4	4.020e-4	1.034e-3	1.382e-3
2560	3.238e-4	1.022e-4	1.023e-4	2.595e-4	6.240e-4
Rate of convergence	1.994	1.972	1.975	2.012	1.147

Table 3.2: Relative errors of AI2*AB3, AM2*AX2*, BDF2BX2*, BI2*BX3* and CNLF-RAW ($\alpha = 0.53, \nu = 0.2$).

due to the CN discretization, yielding third order amplitude and second order phase speed for the physical mode. Linear analysis shows that CNLF-hoRA is unconditionally stable provided that $\omega_H > r_0(\beta)\omega_L$, for some $r_0(\beta) > 0$ that depends on the filter parameter β. We empirically found that $r_0(\beta)$ is uniformly bounded by 2.25. Finally, we presented several numerical tests to verify the convergence of the scheme.

# of time steps	$\beta = 0.1$	$\beta = 0.2$	$\beta = 0.3$	$\beta = 0.4$
320	7.388e-3	8.657e-3	1.031e-2	1.255e-2
640	1.843e-3	2.154e-3	2.555e-3	3.092e-3
1280	4.630e-3	5.403e-4	6.401e-4	7.735e-4
2560	1.218e-4	1.411e-4	1.659e-4	1.992e-4
Rate of convergence	1.926	1.937	1.948	1.957

Table 3.3: Relative errors of CNLF-hoRA with several values of β.

4.0 GENERAL HIGHER-ORDER ROBERT–ASSELIN TYPE TIME FILTERS

In this chapter we introduce the construction of the family of hoRA type time filters that achieve pre-determined order of overall accuracy. Although they may require more memory usages, the in-core memory in many computer systems has significantly increased over the last several years. Therefore, most modest-sized atmospheric models are not limited by lack of memory, and they can easily accommodate the storage needs of the higher-order methods.

We will particularly focus on the fourth-order hoRA filter and investigate its stability and accuracy properties. We then present several numerical experiments (pure oscillation [48] and Lorenz system [10]) to verify the convergence. The work of this chapter is based on [30].

4.1 CONSTRUCTION OF GENERAL HIGHER-ORDER ROBERT–ASSELIN TYPE TIME FILER

To extend the hoRA2(3) filter to more general order of accuracy, we consider the following scheme:

$$v^{n+1} = u^{n-1} + 2i\omega\triangle t v^n, \tag{4.1}$$

$$u^n = v^n + \left(a_{n+1}v^{n+1} + a_n v^n + a_{n-1}u^{n-1} + a_{n-2}u^{n-2} + \cdots + a_{n-k}u^{n-k}\right), \quad k \geq 1. \tag{4.2}$$

Again, v and u are unfiltered and filtered variables, respectively, and a_j, $j = n+1, \ldots, n-k$ are to be determined. Notice that there are $k+2$ degrees of freedom. The analysis below

will show that the scheme could achieve at most $(k+1)$-th order of accuracy. We recall that by the Lax–Richtmyer equivalence theorem, the scheme has to also satisfy the root condition in order to be convergent (see, e.g., [37]).

By a simple calculation, scheme (4.1)-(4.2) is equivalent to the following multistep method:

$$\begin{aligned} &u^{n+1} - (a_{n+1} + a_{n-1})u^n - (1 + a_n + a_{n-2})u^{n-1} - a_{n-3}u^{n-2} - \cdots - a_{n-k}u^{n-k+1} \\ &\quad = 2i\omega\triangle t \left(u^n - a_{n-1}u^{n-1} - a_{n-2}u^{n-2} - \cdots - a_{n-k}u^{n-k}\right). \end{aligned} \tag{4.3}$$

We may verify the consistency by checking that the coefficients satisfy certain algebraic equations, as stated in the following theorem.

Theorem 4.1.1. *The multistep method (4.3) is consistent if and only if the following algebraic relations among the coefficients are satisfied*

$$\sum_{j=-1}^{k} a_{n-j} = 0, \quad \sum_{j=0}^{k} j a_{n-j} = 0. \tag{4.4}$$

Moreover, if the true solution u is smooth, then the scheme is of order $q \le k+1$ if and only if (4.4) holds and the following additional conditions are satisfied

$$a_n + \sum_{j=1}^{k} \left((j-1)^p + 2p \cdot j^{p-1}\right) a_{n-j} = (-1)^p - 1, \quad p = 1, \ldots, q. \tag{4.5}$$

(Note that if $q = 1$ this reduces to the second condition of (4.4).)

Proof. For notational simplicity, we denote $u_i := u(i\triangle t)$, where $u(i\triangle t)$ is the true solution at time $i\triangle t$. Fix a number p, $1 \le p \le q$, then expanding the true solution u_{n-j} in a Taylor series yields

$$u_{n-j} = u_n + \sum_{\ell=1}^{k+2} \frac{(j\triangle t)^\ell}{\ell!} u_n^{(\ell)}.$$

Plugging these values back into (4.3) gives the following coefficient for $(\omega\triangle t)^{p-1}$ in the truncation error:

$$\frac{1}{p!}\left(1 - (1 + a_n + a_{n-2})(-1)^p - \sum_{j=3}^{k} a_{n-j}(-(j-1))^p\right) + \frac{2}{(p-1)!}\sum_{j=1}^{k} a_{n-j}(-j)^{p-1}.$$

Equating the above quantity with zero for $p = 1, \ldots, q$ gives conditions (4.5). The condition (4.4) is also easy to check by the definition of consistency. □

Corollary 4.1.2. *The n-th order hoRA filter combined with the LF scheme satisfies*

$$1+\mathcal{O}[(\omega\triangle t)^m],\ \textit{where}\ \begin{cases} m=n+1,\ \textit{if } n \textit{ is odd;} \\ m\geq n+2,\ \textit{if } n \textit{ is even;} \end{cases}$$

and the phase speed is

$$1+\mathcal{O}[(\omega\triangle t)^\ell],\ \textit{where}\ \begin{cases} \ell\geq n+1,\ \textit{if } n \textit{ is odd;} \\ \ell=n,\ \textit{if } n \textit{ is even.} \end{cases}$$

We now show that the RA and hoRA2(3) filters are members of the family (4.2). To see this, let $k=1$ in (4.2). Then from Theorem 4.1.1, coefficients a_{n+1}, a_n, a_{n-1} should satisfy

$$\begin{pmatrix} 1 & 1 & 1 \\ 0 & 1 & 2 \\ 0 & 1 & 4 \end{pmatrix} \begin{pmatrix} a_{n+1} \\ a_n \\ a_{n-1} \end{pmatrix} = \begin{pmatrix} 0 \\ 0 \\ 0 \end{pmatrix}.$$

The first two rows, i.e.,

$$\begin{aligned} a_{n+1}+a_n+a_{n-1}&=0 \\ a_n+2a_{n-1}&=0 \end{aligned}$$

provide first-order accuracy. Solving the above two equations gives

$$(a_{n+1},a_n,a_{n-1})^T=(\gamma,-2\gamma,\gamma)^T,$$

where $\gamma\in\mathbb{R}$. This yields the traditional RA-filtered LF scheme:

$$\begin{aligned} v^{n+1}&=u^{n-1}+2i\omega\triangle t v^n, \\ u^n&=v^n+\gamma\left(v^{n+1}-2v^n+u^{n-1}\right). \end{aligned}$$

If further the third row of the matrix is being considered, the scheme becomes second-order accurate. However, the coefficients are all found to be zeros and thus the filter is degenerated, i.e., the scheme recovers to LF method.

The hoRA2(3) filter introduced in Chapter 2 corresponds to the case $k = 2$ in (4.2). The algebraic conditions (4.4) and (4.5) yield

$$\begin{pmatrix} 1 & 1 & 1 & 1 \\ 0 & 1 & 2 & 3 \\ 0 & 1 & 4 & 9 \\ 0 & 1 & 6 & 25 \end{pmatrix} \begin{pmatrix} a_{n+1} \\ a_n \\ a_{n-1} \\ a_{n-2} \end{pmatrix} = \begin{pmatrix} 0 \\ 0 \\ 0 \\ -2 \end{pmatrix}.$$

The first three rows of the matrix guarantee the second-order accuracy, and solving this gives

$$(a_{n+1}, a_n, a_{n-1}, a_{n-2})^T = \gamma(1, -3, 3, -1)^T,$$

hence (4.1)-(4.2) become

$$\begin{aligned} v^{n+1} &= u^{n-1} + 2i\omega \triangle t v^n, \\ u^n &= v^n + \gamma \left(v^{n+1} - 3v^n + 3u^{n-1} - u^{n-2} \right). \end{aligned}$$

The third-order accuracy is achieved if in addition the fourth row is included, and one can check that this corresponds to hoRA3 ($\beta = 0.4$).

We may achieve a scheme of order 4 if $k = 3$ in (4.2). Theorem 4.1.1 provides us the following equations for the coefficients:

$$\begin{pmatrix} 1 & 1 & 1 & 1 & 1 \\ 0 & 1 & 2 & 3 & 4 \\ 0 & 1 & 4 & 9 & 16 \\ 0 & 1 & 6 & 25 & 62 \\ 0 & 1 & 8 & 65 & 232 \end{pmatrix} \begin{pmatrix} a_{n+1} \\ a_n \\ a_{n-1} \\ a_{n-2} \\ a_{n-3} \end{pmatrix} = \begin{pmatrix} 0 \\ 0 \\ 0 \\ -2 \\ 0 \end{pmatrix}.$$

This yields

$$a_{n+1} = 15/53, a_n = -56/53, a_{n-1} = 78/53, a_{n-2} = -48/53, a_{n-3} = 11/53,$$

and (4.1)-(4.2) become

$$\begin{aligned} v^{n+1} &= u^{n-1} + 2i\omega \triangle t v^n, \\ u^n &= v^n + \left(\frac{15}{53} v^{n+1} - \frac{56}{53} v^n + \frac{78}{53} u^{n-1} - \frac{48}{53} u^{n-2} + \frac{11}{53} u^{n-3} \right). \end{aligned}$$

Plugging the above parameters in (4.3), the equivalent multistep method writes

$$u^{n+1} - \frac{93}{53}u^n + \frac{51}{53}u^{n-1} - \frac{11}{53}u^{n-2} = 2i\omega\triangle t\left(u^n - \frac{78}{53}u^{n-1} + \frac{48}{53}u^{n-2} - \frac{11}{53}u^{n-3}\right).$$

The corresponding first characteristic polynomial is

$$\rho(r) = r^{n+1} - \frac{93}{53}r^n + \frac{51}{53}r^{n-1} - \frac{11}{53}r^{n-2},$$

and one can check that the norms of non-zero roots are

$$|r_1| = 1, |r_2| = |r_3| = 0.46,$$

hence the root condition is satisfied. Therefore the above scheme is indeed convergent with fourth-order accuracy. In the Section 4.2, we will investigate the scheme's stability, amplitude and phase-speed errors, and present several numerical tests.

We conclude this section with the following algorithm which states the procedure of constructing a hoRA type filter with a pre-determined order of accuracy with minimum degree of freedom.

Algorithm:

Step 1. Set a desired order of accuracy, say $k+1$.

Step 2. Determine the coefficients a_j, $j = n+1, \cdots, n-k$, by solving equations given in (4.4) and (4.5) with $q = k+1$.

Step 3. Check if the root condition is satisfied.

Step 4. If satisfied, plug the coefficients back into (4.1)-(4.2).

4.2 FOURTH ORDER ROBERT–ASSELIN TYPE TIME FILTER

In this section, we perform error and stability analysis of the LF scheme combined with the fourth order hoRA (hoRA4) type time filter that is introduced in the previous section

$$v^{n+1} = u^{n-1} + 2i\omega\triangle t v^n, \tag{4.6}$$

$$u^n = v^n + \left(\frac{15}{53}v^{n+1} - \frac{56}{53}v^n + \frac{78}{53}u^{n-1} - \frac{48}{53}u^{n-2} + \frac{11}{53}u^{n-3}\right). \tag{4.7}$$

4.2.1 Error analysis for amplitude and phase speed

As stated in Section 4.1, scheme (4.6)-(4.7) is equivalent to the following multistep method

$$u^{n+1} - \frac{93}{53}u^n + \frac{51}{53}u^{n-1} - \frac{11}{53}u^{n-2} = 2i\omega\triangle t\left(u^n - \frac{78}{53}u^{n-1} + \frac{48}{53}u^{n-2} - \frac{11}{53}u^{n-3}\right). \tag{4.8}$$

This yields a quartic equation for the amplification factor of LF-hoRA4:

$$A^4 + aA^3 + bA^2 + cA + d = 0, \tag{4.9}$$

where

$$a = -\frac{93}{53} - 2i\omega\triangle t, \quad b = \frac{51}{53} + \frac{156}{53}i\omega\triangle t, \quad c = -\frac{11}{53} - \frac{96}{53}i\omega\triangle t, \quad d = \frac{22}{53}i\omega\triangle t.$$

Equation (4.9) generates one physical mode and three computational modes. Figure 4.1 shows the magnitudes of the amplifications factors, where the solid line is the physical mode and dashed lines are computational modes. In the limit of good time resolution, all computational modes are effectively controlled. Like hoRA2(3) filter, the time step restriction for LF-hoRA4 may be induced from the computational mode as one of the computational modes in hoRA4 is amplified when $\omega\triangle t$ exceeds a number close to 0.6 (see (4.11) in Section 4.2.2).

Turning to the amplitude and phase-speed errors of the physical mode, we find that the amplitude is sixth-order accurate per time step (equivalently, fifth order per unit time)

$$|A_+| - 1 = -1.90(\omega\triangle t)^6 + \mathcal{O}\left[(\omega\triangle t)^8\right],$$

and the phase speed is fourth-order accurate

$$|R_+| - 1 = -0.82(\omega\triangle t)^4 + \mathcal{O}\left[(\omega\triangle t)^6\right].$$

These amplitude and phase-speed errors coincide with the Durran's result [10] given in Proposition 2.1.1, which states that for a method with fourth-order overall accuracy, the numerical solution has at least $\mathcal{O}\left[(\omega\triangle t)^6\right]$ error in amplitude and exactly $\mathcal{O}\left[(\omega\triangle t)^4\right]$ error in phase speed.

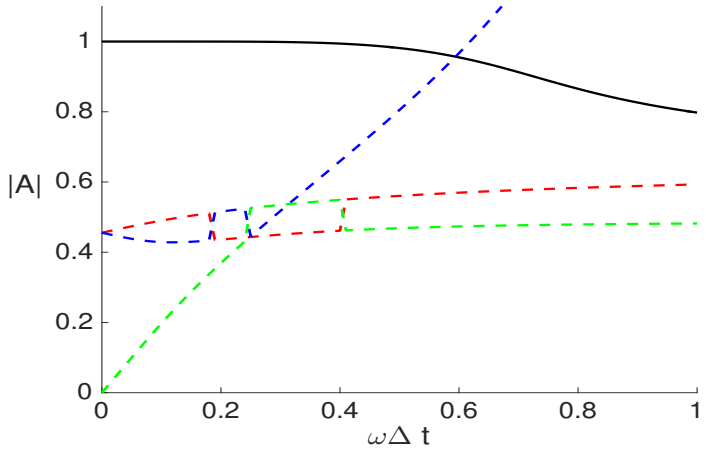

Figure 4.1: Magnitudes of the amplification factors for LF-hoRA4. The solid line represents the physical mode, and dashed lines are computational modes.

4.2.2 Stability

It follows from (4.8) that the characteristic equation for LF-hoRA4 is

$$\zeta^4 - \frac{93}{53}\zeta^3 + \frac{51}{53}\zeta^2 - \frac{11}{53}\zeta - 2z\left(\zeta^3 - \frac{78}{53}\zeta^2 + \frac{48}{53}\zeta - \frac{11}{53}\right) = 0, \tag{4.10}$$

where ζ denotes the points on the unit circle, and $z = i\omega\triangle t$. Plugging $\zeta = e^{i\theta}$ in (4.10), solving for z and letting $\Re(z) = 0$ yields

$$\cos\theta = 1 \text{ or } \cos\theta = 69/1166.$$

Consequently, we find

$$z = 0 \text{ or } z = \pm 0.6186i,$$

which indicates that the root locus curve intersects the imaginary axis of the complex z-plane at $(0, 0)$, $(0, 0.6186i)$ and $(0, -0.6186i)$, as shown in Figure 4.2.

Thus, the stability of LF-hoRA4 is given by

$$\omega\triangle t \leq 0.6186. \tag{4.11}$$

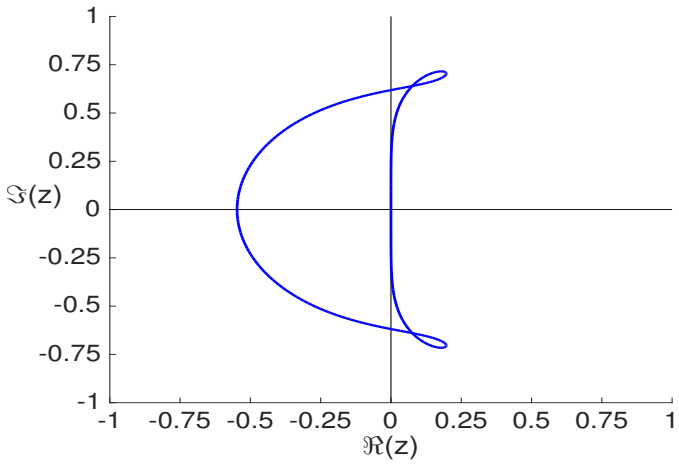

Figure 4.2: Root locus curve of LF-hoRA4. The stability is given by the intersection of the root locus curve with the imaginary axis.

4.2.3 Numerical tests

4.2.3.1 Pure oscillation For a simple linear test problem, we consider the pure oscillation equation

$$F'(t) = i\omega F(t),$$

where $F(t) = \cos\omega t + i\sin\omega t$. We take $\omega = 5$ and numerically integrate the oscillation equation using LF-hoRA3 and LF-hoRA4 over the time interval $0 \leq t \leq 50$. The relative errors are evaluated at the final time, and they are listed in the Table 4.1. As expected, these methods exhibit third-order and fourth-order convergence rates, respectively.

4.2.3.2 Lorenz system As in Section 2.9.2, we consider the Lorenz system

$$\begin{aligned}
\frac{dX}{dt} &= \sigma(Y - X), \\
\frac{dY}{dt} &= -XZ + rX - Y, \\
\frac{dZ}{dt} &= XY - bZ,
\end{aligned}$$

# of time steps	Relative error (hoRA3)	Relative error (hoRA4)
800	9.1615e-1	9.9547e-1
1600	2.5296e-1	1.1809-1
3200	3.5750e-2	7.5946e-3
6400	4.5413e-3	4.7477e-4
Rate of convergence	2.9768	3.9997

Table 4.1: Convergence rate of LF-hoRA3 and LF-hoRA4 when applied to the pure oscillation equation.

with the same parameter values and the initial conditions. The system is numerically integrated over the time interval $[0, 5]$ using LF-hoRA3 and LF-hoRA4. The reference solution is obtained from the explicit RK4 method with step size 0.00005 s. The relative error is evaluated at the final time. Table 4.2 shows the errors with different number of time steps, and it confirms the convergence rates.

# of time steps	Relative error (hoRA3)	Relative error (hoRA4)
300	5.7079e-5	2.8402e-5
400	2.4257e-5	9.7288e-6
500	1.2408e-5	4.0953e-6
600	7.1631e-6	1.9759e-6
Rate of convergence	3.0141	3.9974

Table 4.2: Convergence rate of LF-hoRA3 and LF-hoRA4 when applied to the lorenz system.

4.3 CONCLUSIONS

In this chapter we built a framework for constructing the hoRA type time filter with any pre-determined order of overall accuracy. Although higher-order methods may require more memory usages, yet it is feasible to adopt them in most modest-sized atmospheric modes since the memory in many computer system has been increased significantly during the last several years. Theorem 4.1.1 may be used to determine the coefficients in the filter step (4.2). Following this framework, we have recovered the RA and hoRA2(3) filters, and in particular, we developed a fourth-order filter, hoRA4. We have analyzed the LF-hoRA4 scheme and found that it exhibits fifth-order accuracy in amplitude, and fourth-order accuracy in phase speed. The stability is analyzed using the root locus curve method, and the maximum $\omega\triangle t$ is found to be 0.6186, for which all amplification factors are non-amplified. Finally, two numerical experiments are presents to confirm the rate of convergence.

5.0 SUPPLEMENTAL ANALYSIS FOR EXISTING TIME FILTERS

Paul D. Williams [48] made in 2009 a remarkable improvement to the RA filter, the RAW filter. It is a "simple" modification based on RA (as it only changes one line of code in the legacy codes) with tremendous gain: the RAW filter significantly increases the amplitude and overall accuracy by at least one significant digit. In recognition, RAW has been adopted as the default scheme in several weather and climate models, see [46, 53]. Later, Williams [50] developed two more schemes to further reduce the amplitude error, which is of great interest for the conservation of physical quantities such as energy and mass. In this chapter we present the linear analysis (stability and consistency error) for the schemes proposed by Paul D. Williams, and summarize the properties in Table 5.1. The work of this chapter is based on [25, 28, 31].

5.1 THE RAW-FILTERED LEAPFROG SCHEME

We recall the LF-RAW scheme, introduced in Chapter 2:

$$\begin{aligned} w^{n+1} &= u^{n-1} + 2\triangle t F(v^n), \\ u^n &= v^n + \frac{\nu\alpha}{2}(w^{n+1} - 2v^n + u^{n-1}), \\ v^{n+1} &= w^{n+1} - \frac{\nu(1-\alpha)}{2}(w^{n+1} - 2v^n + u^{n-1}). \end{aligned}$$

The LF-RAW scheme has been implemented and studied in [46, 1, 38, 53, 35, 52, 20], and its behavior in implicit-explicit (IMEX) integrations was analyzed in [49].

To perform the linear analysis, we write LF-RAW equivalently as a linear multistep method

$$u^n - \nu u^{n-1} - (1-\nu)u^{n-2} = i\omega\triangle t\left(\big(2+\nu(\alpha-1)\big)u^{n-1} - \nu\alpha u^{n-2}\right),$$

which allows us to derive the method's truncation error

$$\tau_n(\triangle t) = \left(\frac{1}{2} - \alpha\right)\nu(i\omega\triangle t)u'^n) + \mathcal{O}[(i\omega\triangle t)^2].$$

The amplitude error for the physical mode is

$$|A_+| - 1 = \frac{\nu(1-2\alpha)}{2(2-\nu)}(\omega\triangle t)^2 + \mathcal{O}[(\omega\triangle t)^4],$$

and the phase-speed error is

$$R_+ - 1 = \frac{1+\nu}{3(2-\nu)}(\omega\triangle t)^2 + \mathcal{O}[(\omega\triangle t)^4].$$

The parameter α restores the accuracy that is lost by the RA filter. For example, LF-RAW with $\alpha = 0.53$ gives one more digit of accuracy than LF-RA. In the extreme case when $\alpha = 0.5$, the amplitude is of order $(\omega\triangle t)^4$ per time step, and the overall accuracy becomes second order.

On the other hand, the root locus curve method gives us the stability condition

$$\omega\triangle t \le \frac{1}{\alpha}\sqrt{\frac{(2-\nu)(2\alpha-1)}{2-\nu+2\alpha\nu}}. \tag{5.1}$$

The right-hand side of (5.1) is a decreasing function of α for every fixed ν. In particular, LF-RAW becomes unstable when $\alpha = 0.5$. Therefore, although it is tempting to use the value of $\alpha = 0.5$ for the best numerical accuracy, we may not be able to use this value because of the instability. Indeed, Williams [48] suggests taking values of α in the range of $0.51 - 0.53$ to obtain almost second-order overall accuracy.

5.2 THE RAW-FILTERED COMPOSITE-TENDENCY LEAPFROG SCHEME

Williams proposed a RAW-filtered composite-tendency leapfrog (CTLF-RAW) scheme in [50], which applied to the oscillation equation (2.3) reads

$$\begin{aligned} w^{n+1} &= u^{n-1} + 2i\omega\triangle t(\gamma v^n + (1-\gamma)w^n), \\ u^n &= v^n + \frac{\nu\alpha}{2}(w^{n+1} - 2v^n + u^{n-1}), \\ v^{n+1} &= w^{n+1} - \frac{\nu(1-\alpha)}{2}(w^{n+1} - 2v^n + u^{n-1}). \end{aligned}$$

The new parameter γ specifies the weighting coefficients for the composite tendency. In particular, the CTLF-RAW scheme recovers to LF-RAW when $\gamma = 1$. Although previous work assumed $0 \leq \gamma \leq 1$, here we allow γ to vary outside this range. Note that this scheme is intrusive as it changes the code of LF step. The behavior of the method in IMEX integrations is studied in [2].

The equivalent multistep method of the above system of equations is

$$\begin{aligned} &u^{n+1} - \nu u^n - (1-\nu)u^{n-1} \\ &= i\omega\triangle t\Big((2 - \nu\gamma(1-\alpha))u^n + \nu(2\gamma + \alpha - 2 - 2\alpha\gamma)u^{n-1} + \nu(1-\alpha)(1-\gamma)u^{n-2}\Big). \end{aligned} \tag{5.2}$$

It follows from (5.2) that the truncation error is

$$\begin{aligned} \tau_n(\triangle t) = \left(\frac{1}{2} - \alpha\right)\nu(i\omega\triangle t)u'(t^n) + \frac{1}{6}\left(2 - \nu(7 - 9\alpha) + 6\nu\gamma(1-\alpha)\right)(i\omega\triangle t)^2 u'(t^n) \\ + \frac{\nu}{24}(25 - 28\alpha - 24\gamma + 24\alpha\gamma)(i\omega\triangle t)^3 u'(t^n) + \mathcal{O}(\triangle t^4). \end{aligned}$$

The scheme is generally first-order accurate if $\nu \neq 0$, and second order if $\alpha = 0.5$, as noted by Williams [50]. Further, the method becomes third order if $\alpha = 0.5$ and $\gamma = (5\nu - 4)/(6\nu)$. This third-order scheme would require $\gamma < 0$ if $\nu < 4/5$. Finally, the scheme exhibits fourth-order accuracy if $\alpha = 0.5, \nu = -8$, and $\gamma = 11/12$. This case is of no practical interest because the negative value of ν forces the computational mode to be amplified.

Formula (5.2) yields the following equation for the amplification factor:

$$A^3 - (\nu + (2 - \nu\gamma(1-\alpha))\, i\omega\triangle t)A^2 \\ - (1 - \nu + \nu(2\gamma + \alpha - 2 - 2\alpha\gamma)i\omega\triangle t)A - \nu(1-\alpha)(1-\gamma)i\omega\triangle t = 0. \tag{5.3}$$

The amplitude error for the physical mode is found to be

$$|A_+| - 1 = \frac{\nu(1-2\alpha)}{2(2-\nu)}(\omega\triangle t)^2 + \mathcal{O}\left[(\omega\triangle t)^4\right],$$

yielding first-order amplitude accuracy, independent of γ. When $\alpha = 0.5$, the quadratic term vanishes and the amplitude error becomes

$$|A_+| - 1 = \frac{\nu(4\gamma - 3 + \nu - \nu\gamma)}{4(2-\nu)^2}(\omega\triangle t)^4 + \mathcal{O}\left[(\omega\triangle t)^6\right],$$

which implies the third-order amplitude accuracy. The fourth-order term now depends on γ. Specifically, CTLF-RAW is amplifying when $\gamma > (3-\nu)/(4-\nu)$, and is damping if $\gamma < (3-\nu)/(4-\nu)$. When $\gamma = (3-\nu)/(4-\nu)$, the amplitude error is fifth-order accurate:

$$|A_+| - 1 = \frac{\nu}{4(4-\nu)(2-\nu)^2}(\omega\triangle t)^6 + \mathcal{O}\left[(\omega\triangle t)^8\right].$$

However, the coefficient of the sixth-order term is always positive, implying a slight instability of the scheme.

The phase-speed error, when $\alpha = 1/2$, is

$$R_+ - 1 = \frac{6\nu\gamma + 4 - 5\nu}{12(2-\nu)}(\omega\triangle t)^2 + \mathcal{O}[(\omega\triangle t)^4],$$

and it is fourth-order accurate if further $\gamma = (5\nu - 4)/(6\nu)$.

As for the stability, we focus on the $\alpha = 1/2$ case.[1] Using the root locus curve method, we find that the stability condition is:

$$\omega\triangle t \le \frac{2}{(1-\gamma)(4-\nu)}\sqrt{\frac{(3-\nu)-(4-\nu)\gamma}{1+\nu(1-\gamma)}}, \quad \gamma \le (3-\nu)/(4-\nu).$$

As a result, the scheme becomes unstable when $\gamma = (3-\nu)/(4-\nu)$, which coincides with instability from the amplitude analysis. We note that the third-order scheme ($\gamma = (5\nu - 4)/(6\nu)$) has a stable range for the small, positive values of ν that are used in practical applications.

[1] For the CTLF-RAW method, it is of more interest when $\alpha = 1/2$ since the scheme is at least second-order accurate.

5.3 THE COMPOSITE-TENDENCY LEAPFROG SCHEME WITH A MORE DISCRIMINATING FILTER

In [50], Williams developed a composite-tendency leapfrog scheme with a more discriminating filter (CTLF-D)

$$\begin{aligned} w^{n+1} &= u^{n-1} + 2i\omega\triangle t(\gamma v^n + (1-\gamma)w^n), \\ u^n &= v^n + \nu\alpha(w^{n+1} - 4v^n + 6u^{n-1} - 4u^{n-2} + u^{n-3}), \\ v^{n+1} &= w^{n+1} - \nu(1-\alpha)(w^{n+1} - 4v^n + 6u^{n-1} - 4u^{n-2} + u^{n-3}). \end{aligned}$$

In addition to composite tendency in the LF step, this scheme adopts a filter of the form $(1, -4, 6, -4, 1)$.

The system is equivalent to the following multistep method:

$$\begin{aligned} &u^{n+1} - \nu(4+3\alpha)u^n - (1 - 7\nu - \nu\alpha)u^{n-1} - \nu(4-3\alpha)u^{n-2} + \nu(1-\alpha)u^{n-3} \\ &= 2\left(1 - \nu(1-\alpha)\gamma\right)u^n - \nu\left(8(1-\alpha)(1-\gamma) + 12\alpha\right)u^{n-1} \\ &+ \nu\left(12(1-\alpha)(1-\gamma) + 8\alpha\right)u^{n-2} - \nu\left(8(1-\alpha)(1-\gamma) + 2\alpha\right)u^{n-3} + 2\nu(1-\alpha)(1-\gamma)u^{n-4}, \end{aligned} \tag{5.4}$$

from which one can derive the truncation error:

$$\begin{aligned} \tau_n(\triangle t) = &\frac{1 - \nu(1+2\alpha)}{3}(i\omega\triangle t)^2 u'(t^n) + \frac{\nu(3-5\alpha)}{3}(i\omega\triangle t)^3 u'(t^n) \\ &+ \frac{181\nu - 308\alpha\nu - 120\nu\gamma + 120\alpha\nu\gamma - 1}{60}(i\omega\triangle t)^4 u'(t^n) + \mathcal{O}[(i\omega\triangle t)^5]. \end{aligned}$$

Thus, CTLF-D is second order in general. Further, it could theoretically be third-order accurate if $\alpha = (1-\nu)/(2\nu)$, and even higher order for appropriate values of the parameters which set zero the coefficients of the higher-order terms. However, the root condition is not satisfied in this case. To see this, set $\omega = 0$ and write (5.4) in terms of the amplification factor A:

$$A^4 - \nu(4+3\alpha)A^3 - (1 - 7\nu - \nu\alpha)A^2 - \nu(4-3\alpha)A + \nu(1-\alpha) = 0. \tag{5.5}$$

It turns out that when $\alpha = (1-\nu)/(2\nu)$, equation (5.5) has the root $A = 1$ with multiplicity two, violating the root condition (see e.g., [37]). Indeed, the numerical solution grows linearly

in time, while is supposed to be constant. Thus, the scheme is second-order accurate at all time.

The amplitude error is found to be

$$|A_+| - 1 = -\frac{\nu(1-2\alpha)}{2(1-\nu-2\alpha\nu)}(\omega\triangle t)^4 + \mathcal{O}[(\omega\triangle t)^6],$$

which, by setting $\alpha = 1/2$, becomes

$$|A_+| - 1 = \frac{\nu(5-8\gamma-9\nu+14\nu\gamma)}{8(1-2\nu)^2}(\omega\triangle t)^6 + \mathcal{O}[(\omega\triangle t)^8].$$

Further, the sixth-order term vanishes when $\gamma = (5-9\nu)/(2(4-7\nu))$ and gives the seventh-order amplitude error:

$$|A_+| - 1 = -\frac{5\nu(4-13\nu+11\nu^2)}{32(1-2\nu)^2(4-7\nu)}(\omega\triangle t)^8 + \mathcal{O}[(\omega\triangle t)^{10}].$$

The phase-speed error, in this case, is second order:

$$R_+ - 1 = \frac{1}{6}(\omega\triangle t)^2 + \mathcal{O}[(\omega\triangle t)^4].$$

As shown in the truncation error analysis, CTLF-D is second-order accurate regardless of the parameters. Nevertheless, the amplitude exhibits the highest-order of accuracy when $\alpha = 1/2$ and $\gamma = (5-9\nu)/(2(4-7\nu))$. For this reason, we only consider the stability for these particular values of parameters. The root locus curve method yields that

$$\omega\triangle t \leq \sqrt{1 - \left(\frac{8-45\nu+55\nu^2}{12-20\nu}\right)^2 \frac{8(4-7\nu)(2-5\nu+5\nu^2)}{(4+25\nu-55\nu^2)(16-68\nu+105\nu^2-55\nu^3)}}. \tag{5.6}$$

5.4 SUMMARY

We summarize several properties of Williams' schemes in Table 5.1.

Method	Order	Amplitude	Phase speed	Maximum $\omega\triangle t$
LF-RAW	1 or 2	$1-\frac{\nu(2\alpha-1)}{2(2-\nu)}p^2+\mathcal{O}(p^4)$	$1+\left(\frac{(1-\nu(1-\alpha))(2-\alpha\nu)}{(2-\nu)^2}-\frac{1}{3}\right)p^2$	$\frac{1}{\alpha}\sqrt{\frac{(2-\nu)(2\alpha-1)}{2-\nu+2\alpha\nu}}$
CTLF-RAW	2 or 3	$1+\frac{\nu(4\gamma-3+\nu-\nu\gamma)}{4(2-\nu)^2}p^4+\mathcal{O}(p^6)$	$1+\frac{6\nu\gamma+4-5\nu}{12(2-\nu)}p^2+\mathcal{O}(p^4)$	$\sqrt{\frac{4((3-\nu)-(4-\nu)\gamma)}{(1+\nu(1-\gamma))[(1-\gamma)(4-\nu)]^2}}$
CTLF-D	2	$1-\frac{5\nu(4-13\nu+11\nu^2)}{32(1-2\nu)^2(4-7\nu)}p^8$	$1+\frac{1}{6}p^2$	Formula (5.6)

Table 5.1: Several properties of Williams' schemes. We denote $p=\omega\triangle t$, and amplitude or phase speed that is with $\mathcal{O}(p^k)$ indicates that it is able to be of order up to p^k.

6.0 STABILITY ANALYSIS OF THE CRANK-NICOLSON-LEAPFROG METHOD WITH THE ROBERT–ASSELIN–WILLIAMS TIME FILTER

6.1 INTRODUCTION

The advection-diffusion problems in geophysical fluid dynamics can be written in the following system of differential equations:

$$\frac{du}{dt} + Au = \Lambda u, \tag{6.1}$$

where $u : [0, \infty) \to \mathbb{R}^N$, A and Λ are $N \times N$ matrices such that $A + A^T \geq 0$ and $\Lambda = -\Lambda^T$. When $A + A^T = 0$ the system is exactly conservative for the euclidean norm: $|u(t)| = |u(0)|$. When $A + A^T > 0$ it is dissipative, $|u(t)| \to 0$ as $t \to \infty$.

The CNLF is a commonly used IMEX method for advection-diffusion problems. Stability was proven by Fourier methods in 1963 [21] in 2012 by energy methods for systems, [26]. It was also proven that the unstable or computational mode is stable in [19]. In practical computations with unfiltered CNLF method, however, non-physical growth in the unstable mode is often reported (e.g., [18] and [14, page 242]).

In this chapter we consider the CNLF method with the RAW time filter

$$\frac{w^{n+1} - u^{n-1}}{2\triangle t} = -A\frac{w^{n+1} + u^{n-1}}{2} + \Lambda v^n, \tag{6.2}$$

$$u^n = v^n + \frac{\nu\alpha}{2}(w^{n+1} - 2v^n + u^{n-1}), \tag{6.3}$$

$$v^{n+1} = w^{n+1} + \frac{\nu(\alpha - 1)}{2}(w^{n+1} - 2v^n + u^{n-1}). \tag{6.4}$$

We will perform the stability analysis for the above method. Unlike the scalar case, however, the stability conditions derived from the root locus curve method provide *necessary but not*

sufficient conditions. This is mainly due to the fact that matrices A and Λ do not commute in general. For example, Asher, Ruuth and Wetton [3] page 811 note "*these results provide necessary but not sufficient conditions for stability...*" and Hundsdorfer and Ruuth [17] page 2019 note "*Theoretical results are difficult to obtain if these linearizations do not commute...*".

Therefore, we adopt the energy methods through G-stability theory [7, 15] to derive the sufficient stability condition. The work of this chapter is based on [20].

6.2 G-STABILITY ANALYSIS

The identification of the equivalent multistep method is the first step in the stability analysis.

Theorem 6.2.1. *The approximation u^n of the CNLF method with the RAW filter satisfies*

$$\begin{aligned} u^n - \nu u^{n-1} - (1-\nu)u^{n-2} = &- \triangle t A(u^n + \nu(\alpha-1)u^{n-1} + (1-\nu\alpha)u^{n-2}) \\ &+ \triangle t\Lambda\Big(\big(2+\nu(\alpha-1)\big)u^{n-1} - \nu\alpha u^{n-2}\Big). \end{aligned} \tag{6.5}$$

Proof. This equivalence is proven by algebraic elimination of intermediate variables. Indeed, the first two steps, (6.2) and (6.3), can be rewritten as a block 2x2 system

$$\begin{bmatrix} (I+\Delta tA) & -2\Delta t\Lambda \\ \frac{\nu\alpha}{2}I & (1-\nu\alpha)I \end{bmatrix} \begin{bmatrix} w^{n+1} \\ v^n \end{bmatrix} = \begin{bmatrix} (I-\Delta tA)\,u^{n-1} \\ u^n - \frac{\nu\alpha}{2}u^{n-1} \end{bmatrix}.$$

We solve this system expressing w^{n+1}, v^n in terms of u^n, u^{n-1}. Next these are inserted into (6.4), which completes the proof.

□

For vectors of the same length, denote the usual euclidean inner product and norm by $\langle u, v\rangle := u^T v$, $|u|^2 := \langle u, u\rangle$, the weighted norm by $\|u\|_A^2 := u^T A u$ (well-defined since $A + A^T > 0$), and by $\|\Lambda\|$ the matrix norm of Λ. For notational simplicity, denote γ, p, q, r by

$$\gamma = \nu\sqrt{(1-\alpha)^2 + \alpha^2\triangle t^2\|\Lambda\|^2}, \qquad p = 1 - \frac{\gamma}{2}, \tag{6.6}$$

$$q = 1 - \frac{\gamma}{2} - \nu\left(1 - \frac{\nu}{2}\right), \qquad r = \sqrt{(\gamma-\nu)^2 + ((2-\nu)\triangle t\|\Lambda\|)^2}.$$

There holds $p > r^2/(4q)$ for $\alpha \in [0.5, 1]$ and $\nu \in (0, 1]$. Our main result is as follows.

Theorem 6.2.2. *Consider CNLF-RAW (6.2)-(6.4) with $\alpha \in [0.5, 1]$ and $\nu \in (0, 1]$. Suppose that the time step condition holds*

$$\triangle t\|\Lambda\| \le \sqrt{\frac{(2-\nu)(2\alpha-1)}{\alpha^2(2+\nu-2\alpha\nu)}}\,(1-\nu\,(\alpha-0.5))\,, \tag{6.7}$$

then the method (6.2)-(6.4) is stable. More precisely, for each $N \ge 2$ we have

$$\begin{aligned}
&\Big(p - \frac{r^2}{4q}\Big)|u^n|^2 + \Big(\frac{r}{2\sqrt{q}}|u^n| - \sqrt{q}|u^{n-1}|\Big)^2 \\
&\quad + \frac{\gamma}{2}\sum_{n=2}^{N}\big(|u^n - u^{n-1}| - |u^{n-1} - u^{n-2}|\big)^2 + \Big(\frac{\nu}{2}(2\alpha - \nu(2\alpha-1)) - \gamma\Big)\sum_{n=2}^{N-1}|u^n - u^{n-1}|^2 \\
&\quad + \triangle t\sum_{n=2}^{N}\|u^n + \nu(\alpha-1)u^{n-1} + (1-\nu\alpha)u^{n-2}\|_A^2 \\
&\le |u^1|^2 + |u^0|^2 - (2-\nu)\triangle t\langle \Lambda u^0, u^1\rangle + \frac{\gamma}{2}|u^1 - u^0|^2.
\end{aligned} \tag{6.8}$$

Proof. First, we introduce some notation to simplify the proof.

$$\begin{aligned}
&\eta^n = u^n - u^{n-1}, \\
&x = \frac{1}{2}\sqrt{\frac{\nu}{2}(2+\nu-2\alpha\nu)}, \qquad y = \frac{1}{2}\sqrt{\frac{\nu}{2}(2-\nu)(2\alpha-1)}, \\
&\gamma = \sqrt{4(x^2-y^2)^2 + (\alpha\nu\triangle t\|\Lambda\|)^2}, \quad p = 1 - \frac{\gamma}{2}, \\
&q = 1 - \frac{\gamma}{2} - 4x^2 - \nu^2(\alpha-1), \qquad r = \sqrt{(\nu(\alpha-2) + 2(x^2-y^2) + \gamma)^2 + ((2-\nu)\Delta t\|\Lambda\|)^2},
\end{aligned}$$

$$\text{and} \quad G = \begin{pmatrix} 1-(x+y)^2, & \frac{\nu}{2}(\alpha-2) + 2x(x+y) \\ \frac{\nu}{2}(\alpha-2) + 2x(x+y), & 1-(x+y)^2 - 4x^2 - \nu^2(\alpha-1) \end{pmatrix}.$$

The variables γ, p, q, r are exactly those defined in (6.6). For $\alpha \in [0.5, 1]$ and $\nu \in (0, 1]$, all the variables (except η^n) are non-negative, $x \ge y \ge 0$, and the matrix G is positive definite.

Taking the inner product of (6.5) with $(u^n + \nu(\alpha-1)u^{n-1} + (1-\nu\alpha)u^{n-2})$, we have the following identity.

$$
\begin{aligned}
0 = &\left(\left\| \begin{matrix} u^n \\ u^{n-1} \end{matrix} \right\|_G^2 - (2-\nu)\triangle t \langle \Lambda u^{n-1}, u^n \rangle \right) - \left(\left\| \begin{matrix} u^{n-1} \\ u^{n-2} \end{matrix} \right\|_G^2 - (2-\nu)\triangle t \langle \Lambda u^{n-2}, u^{n-1} \rangle \right) \\
&+ \triangle t \| u^n + \nu(\alpha-1)u^{n-1} + (1-\nu\alpha)u^{n-2} \|_A^2 + |(x+y)u^n - 2xu^{n-1} + (x-y)u^{n-2}|^2 \\
&- \alpha\nu\triangle t \left(\langle \Lambda u^{n-1}, u^n \rangle - \langle \Lambda u^{n-2}, u^n \rangle + \langle \Lambda u^{n-2}, u^{n-1} \rangle \right). \qquad (6.9)
\end{aligned}
$$

It is easy to check that the last two terms in (6.9) are bounded below by

$$
\begin{aligned}
&|(x+y)u^n - 2xu^{n-1} + (x-y)u^{n-2}|^2 - \alpha\nu\triangle t \Big(\langle \Lambda u^{n-1}, u^n \rangle - \langle \Lambda u^{n-2}, u^n \rangle + \langle \Lambda u^{n-2}, u^{n-1} \rangle \Big) \\
&\geq \left(2(x^2+y^2) - \frac{\gamma}{2} \right) |\eta^n|^2 - \frac{\gamma}{2} |\eta^{n-1}|^2 + \frac{\gamma}{2} \big(|\eta^n| - |\eta^{n-1}| \big)^2 - (x-y)^2 \big(|\eta^n|^2 - |\eta^{n-1}|^2 \big).
\end{aligned}
$$

Inserting this inequality into (6.9), we have

$$
\begin{aligned}
&\left(\left\| \begin{matrix} u^n \\ u^{n-1} \end{matrix} \right\|_G^2 - (2-\nu)\triangle t \langle \Lambda u^{n-1}, u^n \rangle - (x-y)^2 |\eta^n|^2 \right) \\
&\quad + \triangle t \| u^n + \nu(\alpha-1)u^{n-1} + (1-\nu\alpha)u^{n-2} \|_A^2 \\
&\quad + \left(2(x^2+y^2) - \frac{\gamma}{2} \right) |\eta^n|^2 - \frac{\gamma}{2} |\eta^{n-1}|^2 + \frac{\gamma}{2} \left(|\eta^n| - |\eta^{n-1}| \right)^2 \\
&\leq \left(\left\| \begin{matrix} u^{n-1} \\ u^{n-2} \end{matrix} \right\|_G^2 - (2-\nu)\triangle t \langle \Lambda u^{n-2}, u^{n-1} \rangle - (x-y)^2 |\eta^{n-1}|^2 \right). \qquad (6.10)
\end{aligned}
$$

Summing (6.10) for $n = 2$ to N and simplifying it gives

$$
\begin{aligned}
&\left(\left\| \begin{matrix} u^N \\ u^{N-1} \end{matrix} \right\|_G^2 - (2-\nu)\triangle t \langle \Lambda u^{N-1}, u^N \rangle + \left((x+y)^2 - \frac{\gamma}{2} \right) |\eta^N|^2 \right) \\
&\quad + \triangle t \sum_{n=2}^{N} \| u^n + \nu(\alpha-1)u^{n-1} + (1-\nu\alpha)u^{n-2} \|_A^2 + \frac{\gamma}{2} \sum_{n=2}^{N} \left(|\eta^n| - |\eta^{n-1}| \right)^2 \\
&\quad + \left(2(x^2+y^2) - \gamma \right) \sum_{n=2}^{N-1} |\eta^n|^2 \\
&\leq \left\| \begin{matrix} u^1 \\ u^0 \end{matrix} \right\|_G^2 - (2-\nu)\triangle t \langle \Lambda u^0, u^1 \rangle + \frac{\gamma}{2} |\eta_1|^2
\end{aligned}
$$

$$\leq |u^1|^2 + |u^0|^2 - (2-\nu)\triangle t\langle \Lambda u^0, u^1\rangle + \frac{\gamma}{2}|\eta_1|^2. \tag{6.11}$$

The first term on the left-hand side of (6.11) is bounded below by

$$\begin{aligned}
&\left\| \begin{matrix} u^N \\ u^{N-1} \end{matrix} \right\|_G^2 - (2-\nu)\triangle t\langle \Lambda u^{N-1}, u^N\rangle + \Big((x+y)^2 - \frac{\gamma}{2}\Big)|\eta^N|^2 \\
&\geq \Big(p - \frac{r^2}{4q}\Big)|u^N|^2 + \left(\frac{r}{2\sqrt{q}}|u^N| - \sqrt{q}|u^{N-1}|\right)^2,
\end{aligned}$$

where $4pq > r^2$ for $\alpha \in [0.5, 1]$ and $\nu \in (0, 1]$. Therefore (6.11) becomes

$$\begin{aligned}
&\Big(p - \frac{r^2}{4q}\Big)|u^N|^2 + \left(\frac{r}{2\sqrt{q}}|u^N| - \sqrt{q}|u^{N-1}|\right)^2 \\
&\quad + \triangle t \sum_{n=2}^{N} \|u^n + \nu(\alpha-1)u^{n-1} + (1-\nu\alpha)u^{n-2}\|_A^2 + \frac{\gamma}{2}\sum_{n=2}^{N}\left(|\eta_n| - |\eta^{n-1}|\right)^2 \\
&\quad + \big(2(x^2+y^2) - \gamma\big)\sum_{n=2}^{N-1}|\eta^n|^2 \\
&\leq |u^1|^2 + |u^0|^2 - (2-\nu)\triangle t\langle \Lambda u^0, u^1\rangle + \frac{\gamma}{2}|\eta_1|^2.
\end{aligned} \tag{6.12}$$

Under the time step condition (6.7), all terms on the left-hand side of (6.12) are positive. Finally, we write (6.12) in terms of α, ν and u^n to obtain the energy bound (6.8). This concludes the proof. □

Corollary 6.2.3. *When $\alpha = 1$ the resulting CNLF method with the RA filter with $\nu \in (0, 1]$ is stable if*

$$\triangle t\|\Lambda\| \leq 1 - \nu/2.$$

Theorem 6.2.2 implies the control of the unstable mode when $A + A^T > 0$.

Corollary 6.2.4. *Assume $A + A^T > 0$ and the time step condition (6.7) holds. Then the approximations generated by CNLF-RAW satisfy $u^n \to 0$ as $n \to \infty$.*

Proof. The right-hand side of (6.8) is independent of N. Thus, letting $N \to \infty$, the infinite series on the left-hand side of (6.8) converge. Hence, the n-th terms of all three series must approach zero as $n \to \infty$. Since $A + A^T > 0$, as $n \to \infty$ this implies

$$\begin{aligned} a_n &:= u^n - u^{n-1} \to 0, \\ b_n &:= u^n + \nu(\alpha - 1)u^{n-1} + (1 - \nu\alpha)u^{n-2} \to 0. \end{aligned}$$

As a result, we have

$$u^{n-1} = (b_n - \nu\alpha a_{n-1} - (a_n - a_{n-1}))/(2 - \nu) \to 0 \quad \text{as} \quad n \to \infty,$$

which completes the proof. □

Remark 4.1 In the case when $\Lambda = 0$ and A is symmetric positive definite, there holds

$$\left\| \begin{array}{c} u^n \\ u^{n-1} \end{array} \right\|_G \leq R(\triangle tA) \left\| \begin{array}{c} u^{n-1} \\ u^{n-2} \end{array} \right\|_G^2,$$

where $0 < R(\triangle tA) < 1$ for any $\triangle t > 0$.

Proof. If $\Lambda = 0$, without loss of generality, let A be a diagonal matrix, i.e.,

$$A = \text{diag}(\lambda_1, \cdots, \lambda_N), \quad \lambda_k > 0, \quad k = 1, 2, \cdots, N.$$

Then we can analyze the system in terms of components. One can derive that the k-th component of the numerical solution satisfies $u_{(k)}^n = R(\triangle t\lambda_k)u_{(k)}^{n-1}$, where

$$R(\triangle t\lambda_k) = \frac{(\nu + \nu(1-\alpha)\triangle t\lambda_k) \pm \sqrt{(\nu + \nu(1-\alpha)\triangle t\lambda_k)^2 + 4(1 + \triangle t\lambda_k)(1 - \nu - (1 - \nu\alpha)\triangle t\lambda_k)}}{2(1 + \triangle t\lambda_k)}.$$

This yields

$$\left\| \begin{array}{c} u_{(k)}^n \\ u_{(k)}^{n-1} \end{array} \right\|_G = |R(\triangle t\lambda_k)| \left\| \begin{array}{c} u_{(k)}^{n-1} \\ u_{(k)}^{n-2} \end{array} \right\|_G^2.$$

It is easy to check that $|R(\triangle t\lambda_k)| < 1$ for $k = 1, \cdots, N$. By letting

$$R(\triangle tA) = \max_{1 \leq k \leq N} |R(\triangle t\lambda_k)|,$$

we conclude the proof. □

6.3 CONCLUSIONS

In this chapter, we focused on the CNLF-RAW method for system of advection-diffusion equations. The matrices A and Λ do not commute in general, and therefore, we derived the stability using the G-stability theory. In addition, we showed that the RAW filter stabilizes the unstable mode of the CNLF method.

7.0 CONCLUSIONS AND FUTURE WORK

The major contribution of this work is the development and analysis of the family of hoRA time filters for weather and climate models. Their behavior has been investigated in fully explicit and/or implicit-explicit integrations. Compared with the traditional RA filter, hoRA type filters significantly reduce the time-stepping errors and increase the accuracy of the numerical simulation. In addition, our filters have substantial algorithmic advantages. On one hand, they are non-intrusive linear post processes and thus easily implementable in legacy codes. On the other hand, the leapfrog scheme combined with these filters require only one evaluation of the tendency equations. In this way our filters reduce the technical costs and programming effort, compared with other higher-order methods which are either intrusive or require more than one function evaluations.

The main disadvantage of hoRA filters is the memory usages. It has been shown from their construction that more historical variables are required in order to obtain higher-order accuracy. This is troublesome if storage is the main concern. Also, although it has not proven in a rigorous manner, the stability region of the imaginary axis decreases as the filter's accuracy increases, based on the analysis of the second-, third- and fourth-order hoRA filters. Schemes with strong stability properties are still in need in many cases. Thirdly, when splitting waves is being considered, the filtered CNLF method remains second order theoretically, regardless of the filter's own accuracy. This is due to the fact that the Crank-Nicolson discretization is only second order. Therefore, it is an open problem whether or not to adopt a more than second order hoRA filter in the implicit-explicit integrations, at the price of increased memory usages.

The following future projects would provide a deeper understanding about the hoRA filters:

1. Implementing LF-hoRA2(3) in practical operational and/or research climate models. We want to verify if the output is consistent with the theoretical results when used in highly complex models.
2. Implementing CNLF-hoRA in the practical climate models. In particular, we are interested in the performance of the hoRA3 (or hoRA4) filter(s) versus that of hoRA2. This would possibly explain whether there is a need to use more than second-order hoRA filters with the CNLF method.
3. Analyzing the fourth-order hoRA filter that is constructed with one degree of freedom, i.e., $k = 4$ in (4.2). By tweaking the free coefficient, we want to see if we could achieve $\mathcal{O}\left[(\omega \triangle t)^8\right]$ amplitude error.

BIBLIOGRAPHY

[1] J. Amezcua, E. Kalnay, and P. D. Williams, *The effects of the RAW filter on the climatology and forecast skill of the SPEEDY model*, Mon. Wea. Rev., 139 (2011), pp. 608–619.

[2] J. Amezcua and P. D. Williams, *The composite-tendency robert–asselin–williams (raw) filter in semi-implicit integrations*, Quarterly Journal of the Royal Meteorological Society, 141 (2015), pp. 764–773.

[3] U. M. Ascher, S. J. Ruuth, and B. T. R. Wetton, *Implicit-explicit methods for time-dependent partial differential equations*, SIAM J. Numer. Anal., 32 (1995), pp. 797–823.

[4] R. Asselin, *Frequency filter for time integrations*, Mon. Wea. Rev., 100 (1972), pp. 487–490.

[5] R. Bleck, *Short-range prediction in isentropic coordinates with filtered and unfiltered numerical models*, Mon. Wea. Rev., 102 (1974), pp. 813–829.

[6] E. Cordero and A. Staniforth, *A problem with the Robert–Asselin time filter for three-time-level semi-implicit semi-lagrangian discretizations*, Mon. Wea. Rev., 132 (2004), pp. 600–610.

[7] G. Dahlquist, *G-stability is equivalent to A-stability*, BIT, 18 (1978), pp. 384–401.

[8] R. Daley, C. Girard, J. Henderson, and I. Simmonds, *Short-term forecasting with a multilevel spectral primitive equation model part I - model formulation*, Atmosphere, 14 (1976), pp. 98–116.

[9] M. Déqué and D. Cariolle, *Some destabilizing properties of the Asselin time filter*, Mon. Wea. Rev., 114 (1986), pp. 880–884.

[10] D. R. Durran, *The third-order Adams-Bashforth method: An attractive alternative to leapfrog time differencing*, Mon. Wea. Rev., 119 (1991), pp. 702–720.

[11] ——, *Numerical methods for fluid dynamics*, vol. 32 of Texts in Applied Mathematics, Springer, New York, second ed., 2010. With applications to geophysics.

[12] D. R. Durran and P. N. Blossey, *Implicit-Explicit Multistep Methods for Fast-Wave-Slow-Wave Problems*, Mon. Wea. Rev., 140 (2012), pp. 1307–1325.

[13] C. T. Gordon and W. F. Stern, *A description of the GFDL global spectral model*, Mon. Wea. Rev., 110 (1982), pp. 625–644.

[14] P. Gresho, R. Sani, and M. Engelman, *Incompressible flow and the finite element method: advection-diffusion and isothermal laminar flow*, Incompressible Flow & the Finite Element Method, Wiley, 1998.

[15] E. Hairer and G. Wanner, *Solving ordinary differential equations. II*, vol. 14 of Springer Series in Computational Mathematics, Springer-Verlag, Berlin, 2010. Stiff and differential-algebraic problems, Second revised edition.

[16] G. J. Haltiner and J. M. McCollough, *Experiments in the initialization of a global primitive equation model*, J. Appl. Meteor., 14 (1975), pp. 281–288.

[17] W. Hundsdorfer and S. J. Ruuth, *IMEX extensions of linear multistep methods with general monotonicity and boundedness properties*, J. Comput. Phys., 225 (2007), pp. 2016–2042.

[18] W. Hundsdorfer and J. Verwer, *Numerical solution of time-dependent advection-diffusion-reaction equations*, vol. 33 of Springer Series in Computational Mathematics, Springer-Verlag, Berlin, 2003.

[19] N. Hurl, W. Layton, Y. Li, and M. Moraiti, *The unstable mode in the crank-nicolson leap-frog method is stable*, to appear in Int. J. Numer. Anal. Model., (2016).

[20] N. Hurl, W. Layton, Y. Li, and C. Trenchea, *Stability analysis of the Crank–Nicolson-Leapfrog method with the Robert–Asselin–Williams time filter*, BIT, 54 (2014), pp. 1009–1021.

[21] O. Johansson and H.-O. Kreiss, *Überdas Verfahren der zentralen Differenzen zur Lösung des Cauchy problems für partielle Differentialgleichungen*, Nordisk Tidskr. Informations-Behandling, 3 (1963), pp. 97–107.

[22] S. K. Kar, *A semi-implicit Runge–Kutta time-difference scheme for the two-dimensional shallow-water equations*, Mon. Wea. Rev., 134 (2006), pp. 2916–2926.

[23] Y. Kurihara, *On the use of implicit and iterative methods for the time integration of the wave equation*, Mon. Wea. Rev., 93 (1965), pp. 33–46.

[24] M. Kwizak and A. J. Robert, *A semi-implicit scheme for grid point atmospheric models of the primitive equation*, Mon. Wea. Rev., 99 (1971), pp. 32–36.

[25] W. Layton, Y. Li, and C. Trenchea, *Recent developments in IMEX methods with time filters for systems of evolution equations*, J. Comput. Appl. Math., 299 (2016), pp. 50–67.

[26] W. Layton and C. Trenchea, *Stability of two IMEX methods, CNLF and BDF2-AB2, for uncoupling systems of evolution equations*, Appl. Numer. Math., 62 (2012), pp. 112–120.

[27] Y. Li and C. Trenchea, *A higher-order Robert–Asselin type time filter*, J. Comput. Phys., 259 (2014), pp. 23–32.

[28] ——, *Analysis of time filters used with the leapfrog scheme*, in Coupled Problems in Science and Engineering VI COUPLED PROBLEMS 2015, E. O. n. B. Schrefler and M. Papadrakakis, eds., Venice, Italy, May 18-20 2015, International Center for Numerical Methods in Engineering (CIMNE), pp. 1261–1272.

[29] ——, *A higher order Robert-Asselin type time filter in the semi-explicit integrations*, tech. rep., University of Pittsburgh, 2015.

[30] ——, *The fourth-order Robert-Asselin type time filter*, tech. rep., University of Pittsburgh, 2016.

[31] Y. Li and P. D. Williams, *Analysis of the RAW filter in composite-tendency leapfrog integrations*, tech. rep., University of Pittsburgh, 2014.

[32] D. Lilly, *On the computational stability of numerical solutions of time-dependent non-linear geophysical fluid dynamics problems*, Mon. Wea. Rev., 93 (1965), pp. 11–25.

[33] P. Lynch, *The swinging spring: A simple model for atmospheric balance, in largescale atmosphereocean dynamics: Vol II: Geometric methods and models*, Cambridge University Press, (2002), pp. 64–108.

[34] L. Magazenkov, *Trudy Glavnoi Geofizicheskoi Observatorii*, (Transactions of the Main Geophysical Observatory), 410 (1980), pp. 120–129.

[35] N. Oger, O. Pannekoucke, A. Doerenbecher, and P. Arbogast, *Assessing the influence of the model trajectory in the adaptive observation Kalman filter sensitivity method*, Q. J. R. Meteorol. Soc, 138 (2012), pp. 813–825.

[36] R. L. Pfeffer, I. M. Navon, and X. Zou, *A comparison of the impact of two time-differencing schemes on the NASA-GLAS climate model*, Mon. Wea. Rev., 120 (1992), pp. 1381–1393.

[37] A. Quarteroni, R. Sacco, and F. Saleri, *Numerical mathematics*, vol. 37 of Texts in Applied Mathematics, Springer-Verlag, Berlin, second ed., 2007.

[38] D. Ren and L. M. Leslie, *Three positive feedback mechanisms for ice-sheet melting in a warming climate*, J. Glaciol., 57 (2011), pp. 1057–1066.

[39] A. Robert and M. Lépine, *An anomaly in the behaviour of the time filter used with the leapfrog scheme in atmospheric models*, Atmosphere-Ocean, 35 (1997), pp. S3–S15.

[40] A. J. Robert, *The integration of a low order spectral form of the primitive meteorological equations*, J. Met. Soc. Japan, 44, Ser. 2 (1966), pp. 237–245.

[41] ——, *The integration of a spectral model of the atmosphere by the implicit method*, Proc. WMO-IUGG Symp. on NWP, Tokyo, Japan Meteorological Agency, (1969), pp. 19–24.

[42] D. Ruprecht and R. Speck, *Spectral deferred corrections with fast-wave slow-wave splitting*, arXiv preprint arXiv:1602.01626, (2016).

[43] R. E. Schlesinger, L. W. Uccellini, and D. R. Johnson, *The effects of the Asselin time filter on numerical solutions to the linearized shallow-water wave equations*, Mon. Wea. Rev., 111 (1983), pp. 455–467.

[44] A. Staniforth and J. Côté, *Semi-lagrangian integration schemes for atmospheric models-a review*, Mon. Wea. Rev., 119 (1991), pp. 2206–2223.

[45] J. Teixeira, C. Reynolds, and K. Judd, *Time step sensitivity of nonlinear atmospheric models: numerical convergence, truncation error growth, and ensemble design*, J. Atmos. Sci, 64 (2007), p. 175189.

[46] M. Watanabe and Coauthors, *Improved climate simulation by MIROC5: Mean states, variability, and climate sensitivity*, J. Climate, 23 (2010), pp. 6312–6335.

[47] J. S. Whitaker and S. K. Kar, *Implicit-explicit Runge-Kutta methods for fast-slow wave problems*, Mon. Wea. Rev., 141 (2013), pp. 3426–3434.

[48] P. D. Williams, *A proposed modification to the Robert–Asselin time filter*, Mon. Wea. Rev., 137 (2009), pp. 2538–2546.

[49] P. D. Williams, *The RAW filter: An improvement to the Robert–Asselin filter in semi-implicit integrations*, Mon. Wea. Rev., 139 (2011), pp. 1996–2007.

[50] P. D. Williams, *Achieving seventh-order amplitude accuracy in leapfrog integrations*, Mon. Wea. Rev., 141 (2013), pp. 3037–3051.

[51] D. L. Williamson, *Description of NCAR Community Climate Model (CCM0B)*, NCAR Tech. Note NCAR/TN-210 STR, 88 (1983).

[52] C.-C. Young, Y.-C. Liang, Y.-H. Tseng, and C.-H. Chow, *Characteristics of the RAW-filtered leapfrog time-stepping scheme in the ocean general circulation model*, Mon. Wea. Rev., 142 (2013), pp. 434–447.

[53] C.-C. Young, Y.-H. Tseng, M.-L. Shen, Y.-C. Liang, M.-H. Chen, and C.-H. Chien, *Software development of the TaIwan Multi-scale Community Ocean Model (TIMCOM)* , Environ. Modell. Software, 38 (2012), pp. 214 – 219.

[54] S. Zalesak, *Fully multidimensional flux-corrected transport algorithms for fluids*, J. Comput. Phys., 31 (1979), pp. 335–362.

[55] B. Zhao and B. Zhang, *Comparison of different order adams-bashforth methods in an atmospheric general circulation model*, Acta Meterol. Sin., 25 (2011), pp. 754–764.